 CMC, vol.33, no.2, pp.111-154, 2013

SGBEM Voronoi Cells (SVCs), with Embedded Arbitrary-Shaped Inclusions, Voids, and/or Cracks, for Micromechanical Modeling of Heterogeneous Materials

Leiting Dong[1,2] **and Satya N. Atluri**[1,3]

Abstract: In this study,SGBEM Voronoi Cells (SVCs), with each cell representing a grain of the material at the micro-level, are developed for direct micromechanical numerical modeling of heterogeneous composites. Each SVC can consist of either a (each with a different) homogenous isotropic matrix, and can include micro-inhomogeneities such as inclusions, voids of a different material, and cracks. These inclusions and voids in each SVC can be arbitrarily-shaped, such as circular, elliptical, polygonal, etc., for 2D problems. Further, the cracks in each SVC can be fully-embedded, edge, branching, or intersecting types, with arbitrary curved shapes. By rearranging the weakly-singular boundary integral equations, a stiffness matrix and a force vector are developed for each SVC with inclusions, voids, and micro-cracks. The stiffness matrix of each SVC is symmetric, positive semi-definite, and has the correct number of rigid-body modes. The stiffness matrix of each SVC and the force vector can also be interpreted to have the same physical meaning as in traditional displacement finite elements, and related to strain energy and the work done. Therefore, the direct coupling of different SVCs (each with a different isotropic material property, and each with heterogeneities of a different material), or the coupling of SVCs with other traditional or special elements, can be achieved by the usual assembly procedure. Moreover, because the heterogeneous micro-structures are modeled directly in the most natural way, as in the present work, by using an SVC to model each grain, one not only saves the labor of meshing and re-meshing, but also reduces the computational burden by several orders of magnitude as compared to the usual FEM. Through several numerical examples, we demonstrate that the SVCs are useful in not only estimating the overall stiffness properties of heterogeneous composite materials, but they are most useful in capturing the local stress concentrations and singularities in each grain, which act

[1] Center for Aerospace Research & Education, University of California, Irvine
[2] Department of Engineering Mechanics, Hohai University
[3] Distinguished Adjunct-Professor of Multi-Disciplinary Engineering and Computer Science, King Abdulaziz University, Saudi Arabia

as damage precursors, efficiently. Several examples of interaction of cracks with inclusions and voids within each SVC (or material grain) are also presented. Accurate results are obtained for stress intensity factors. Non-collinear fatigue growth of micro-cracks in heterogeneous materialis also modeled very efficiently, with these SVCs, without a need for the complicated re-meshing as is common when using the traditional displacement-based finite element methods.

Keywords: SGBEM Voronoi Cell, SGBEM, matrix, inclusion, void, cracks, fatigue, heterogeneous material

1 Introduction

In recent decades,the wide applications of heterogeneous (composite) materials have grown very rapidly in mechanical, aerospace and defense industries. For example, metals/alloys with precipitates/pores, and metal/polymer/ceramic composite materials with fiber/whisker/particulate reinforcements are of particular interest. In addition to these complexities such as inclusions and voids, defects such as cracks are also commonly observed in heterogeneous materials, caused by manufacturing imperfections, thermal effects, local chemical reactions, etc. The development of efficient and accurate tools to model the micromechanical and macromechanical behavior of heterogeneous materials from the bottom-up and top-down is of fundamental interest in engineering and science.

There are several widely-used analytical tools to predict the overall stiffness properties of heterogeneous materials. For example, [Hashin and Shtrikman (1963)] developedvariational methods to estimate the upper and lower bounds of the elasticity or compliance tensor. [Hill (1965)] developed a self-consistent approach to estimate the homogenized material properties. For a useful reference, one can refer to the book [Nemat-Nasser and Hori (1999)]. Analytical methods have their unique values in the study of micromechanics. However, most of these methods follow the work of an ellipsoidal inclusion in an infinite body, as in [Eshelby (1957)], the work of 2D straight cracks in [Muskhelishvili (1954)], and the work of 3D elliptical flat cracks in [Green and Sneddon(1950), and Vijayakumar and Atluri (1981)]. It is expected that these methods can only accurately model materials with very simple microstructures.

Computational methods have also become popular in the past several decades, for direct numerical modeling of microstructuresof heterogeneous (composite) materials. One of the most popular tools is the finite element method. However, in spite of the manycommercial finite element software available today, it is difficult to model microstructures with inclusions, voids and cracks using off-the-shelf FEM software. This is mainly because of two reasons: the inefficiency to approximate

high-gradients and singular fields with simple polynomial shape functions, and the extremely heavy burden for meshing and re-meshing. For example, materials with fibers, whiskers, particles, and cavities have been studied by [Christman, Needleman and Suresh (1989), Bao, Hutchinson, McMeeking(1991), Guedes and Kikuchi (1991)] and many others. Most of these studies use a Unit Cell model because of the complexity of meshing and the burden of computation. As for microstructures with both inclusions and cracks, very little work has been done by using FEM, see [Li andChudnovsky (1993), LipetzkyandSchmauder(1994), Lipetzky and Knesl(1995)] for some example.

In order to reduce the burden of computation and meshing, Voronoi Cell Finite elements (VCFEMs) were developed by [Ghosh and Mallett (1994); Ghosh, Lee and Moorthy (1995); Ghosh, Lee and Moorthy (2004)], based on the hybrid stress model, the originality of which is due to [Pian (1964)]. However, the completeness of the stress fields generated by polynomial Airy's stress functions or Maxwell's stress functions is of obvious questionability. Incomplete stress field assumptions lead to very poor results of computed stress/strain fields. For detailed discussion of completeness, see [Muskhelishvili (1954), Dong and Atluri (2012a)] for 2D problems, and [Lurie (2005)] for 3D problems. Also, the hybrid-stress method of Pian, and the Voronoi Cell FEM by Ghosh et al. based on the Pian's approach, suffer from the so-called LBB stability conditions, the satisfaction of which is necessary to obtain a stable solution, and such satisfaction has never been correctly addressed in all the literature, including in the papers of Ghosh and his co-workers. Thus, the effectiveness of the VCFEM of Ghosh and Mallett (1994); Ghosh, Lee and Moorthy (1995); Ghosh, Lee and Moorthy (2004)] in computational micromechanics is highly questionable

In a different way, [Moës, Dolbow and Belytschko (1999), Sukumar, Chopp, Moës, and Belytschko (2000)] developed what they call the XFEM, to model cracks and inhomogeneities. Although XFEM became extremely popular in the last few years, its advantages, if any, over the traditional FEM in problems involving inclusions, voids, and cracks, and their growth and /or propagation, is very minimal at best.This will be discussed in detail in two forthcoming papers by the authors [Dong and Atluri (2013b,c)].

In a series of papers in [Dong and Atluri (2011a,b, 2012b,c,d)], a different computational tool was developed—termed ***TreffzVoronoi Cells***(TVCs), which are extremely efficient and accurate for micromechanical modeling of heterogeneous materials. The Trefftz Voronoi Cells were developed using a complete Trefftz trial displacement field (which satisfies exactly the governing differential equations), by using complex variables and conformal mapping method in 2D problems, and Papkovich-Neuber solutionsand spherical/ellipsoidal harmonics for 3D problems.

Only boundary integrals are needed in developing the element stiffness matrices, making TVCs to be computationally extremely efficient. Also because of the completeness of the exact trial displacement fields, accurate stress concentrations near elastic / rigid inclusions and voids in each grain of the material can be determined exactly. Thus, in addition to predicting the overall stiffness properties of heterogeneous composites very accurately and efficiently, the TVCs are extremely useful in predicting damage initiation at the micro-level in heterogeneous composites.

However, as pointed out by [Dong and Atluri (2012a)], it is computationally inconvenient to develop a complete Trefftz trial function field for *arbitrary-shaped* inclusions and voids which are neither circular nor elliptical (or spherical/ellipsoidal).One way is to use multiple source points instead of only one [see Dong and Atluri (2012a)]. It is also difficult to develop complete trial functions for TVCs with non-collinear or non-planar cracks. Therefore, to surmount these difficulties, we develop in the present paper, a SGBEM Voronoi Cell (SVC), to model each grain of a composite material, which may contain totally arbitrarily-shaped inclusions/voids/cracks, for micromechanical modeling of heterogeneous composites.

SVCs are developed in this study by rearranging the weakly-singular boundary integral equations in [Han and Atluri (2003), Dong and Atluri (2013a)]. Each SVC which contains inclusions/voids/cracks has a stiffness matrix and a force vector. The stiffness matrix is symmetric, positive semi-definite, and has the correct number of rigid-body modes. A direct coupling of different SVCs, each cell with different isotropic elastic properties, can be achieved by the usual assembly procedure. The present SVCs not only save the labor of meshing and re-meshing, but also reduce the computational burden by several orders of magnitude, as compared to the usual FEM or even the widely-popular XFEM. Through several numerical examples, we demonstrate that the SVCs can not only estimate the overall stiffness of composite heterogeneous materials, but can also capture the local stress concentrations/singularities/discontinuities exactly and efficiently. Several examples of interaction of microcracks with inclusions and voids are also presented. Accurate results are obtained for stress intensity factors. Non-collinear fatigue growth of micro-cracks in heterogeneous composite material is efficiently modeled, without the need for complicated re-meshing as in traditional displacement finite elements. The present methods will also be shown to be far more superior in accuracy as well as human and computational costs, as compared to the XFEM [Moës, Dolbow, and Belytschko (1999), and the thousands of papers on XFEM in the literature since then], or the peridynamic methods.

The rest of this paper is organized as follows: in section 2, we review the weakly-singular boundary integral equations for 2D problems; in section 3, we rearrange the BIEs to develop the stiffness matrix and force vector of the SVCs with arbi-

trarily shaped inclusions/voids, but without cracks; in section 4, we develop SVCs with arbitrarily shaped inclusions/voids, and cracks; in section 5, we demonstrate the power of the present SVC method through several numerical examples of micromechanics; in section 6, we complete this paper with some concluding remarks.

2 Weakly-Singular Symmetric Galerkin Boundary Integral Equations for Plane Elasticity

Consider a linear elastic solid undergoing infinitesimal elasto-static deformations. Cartesian coordinates ξ_i identify a material particle in the solid; and Cartesian coordinates x_i identify the source point of the 2D Kelvin's solution, see Fig. 1. $\sigma_{ij}, \varepsilon_{ij}, u_i$ are Cartesian components of the stress tensor, strain tensor and displacement vector of the deformable solid, respectively. $\bar{f}_i$ are the components of the body force. We use $()_{,i}$ to denote differentiation with respect to ξ_i; and use $\frac{\partial}{\partial x_i}$ to denote differentiation with respect to x_i. The governing differential equation of the solid can be written in terms of displacements:

$$\left[E_{ijkl} u_{k,l}(\boldsymbol{\xi})\right]_{,i} + \bar{f}_j = 0 \tag{1}$$

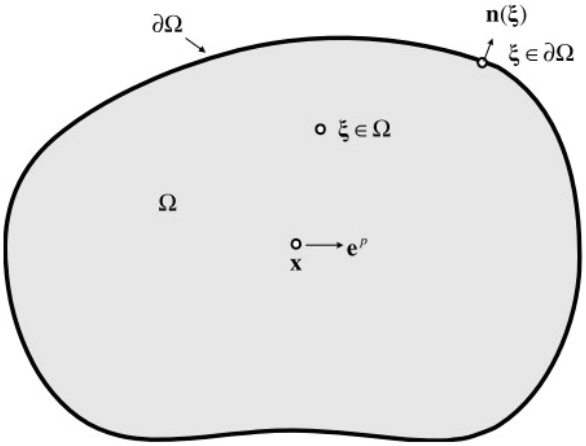

Figure 1: A solution domain with the source point **x** and the material point $\boldsymbol{\xi}$, taken from [Han and Atluri (2003)]

For isotropic plane elasticity,

$$E_{ijkl} = \mu\left(\frac{2\bar{v}}{1-2\bar{v}}\delta_{ij}\delta_{kl} + \delta_{ik}\delta_{jl} + \delta_{il}\delta_{jk}\right) \; i,j,k,l = 1,2$$
$$\bar{v} = \begin{cases} v & \text{for plane strain problems} \\ \frac{v}{1+v} & \text{for plane stress problems} \end{cases} \tag{2}$$

where μ, v are the shear modulus and Possion's ratio, respectively, of the isotropic solid.

Using $u_j^{*p}(\mathbf{x},\boldsymbol{\xi})$, the 2D Kelvin's solution for displacements, as the test functions, we write the weak-form of (1), as:

$$\int_\Omega \left\{ \left[E_{ijkl}u_{k,l}(\boldsymbol{\xi})\right]_{,i} + \bar{f}_j(\boldsymbol{\xi}) \right\} u_j^{*p}(\mathbf{x},\boldsymbol{\xi})\, d\Omega_{\boldsymbol{\xi}} = 0 \tag{3}$$

wherethe 2D Kelvin's solution satisfies the equation:

$$\sigma_{ij,i}^{*p}(\mathbf{x},\boldsymbol{\xi}) = \left[E_{ijkl}u_{k,l}^{*p}(\mathbf{x},\boldsymbol{\xi})\right]_{,i} = -\delta_{jp}(\mathbf{x},\boldsymbol{\xi}) \tag{4}$$

where $\delta_{jp}(\mathbf{x},\boldsymbol{\xi}) = \delta_{jp}\delta(\mathbf{x},\boldsymbol{\xi})$ is a product of the Kronecker delta and the Dirac delta function in space.

Using the divergence theorem twice, we obtain the traditional displacement BIE:

$$\begin{aligned} Cu_p(\mathbf{x}) = &\int_{\partial\Omega} t_j(\boldsymbol{\xi})u_j^{*p}(\mathbf{x},\boldsymbol{\xi})dS_{\boldsymbol{\xi}} - \int_{\partial\Omega} u_j(\boldsymbol{\xi})t_j^{*p}(\mathbf{x},\boldsymbol{\xi})dS_{\boldsymbol{\xi}} \\ &+ \int_\Omega \bar{f}_j(\boldsymbol{\xi})u_j^{*p}(\mathbf{x},\xi)d\Omega_{\boldsymbol{\xi}} \end{aligned} \tag{5}$$

where

$$C = \begin{cases} 1 & \text{for } \mathbf{x} \in \Omega \\ \frac{1}{2} & \text{for } \mathbf{x} \in \partial\Omega \\ 0 & \text{else} \end{cases} \tag{6}$$

Similarly, using the gradient of the Kelvin's displacement fundamental solution, namely, $u_{j,k}^{*p}(\mathbf{x},\boldsymbol{\xi})$, as the test function, we write the vector weak-form of (1), as:

$$\int_\Omega \left\{ \left[E_{ijmn}u_{m,n}(\boldsymbol{\xi})\right]_{,i} + \bar{f}_j(\boldsymbol{\xi}) \right\} u_{j,k}^{p}(\mathbf{x},\boldsymbol{\xi})\, d\Omega_{\boldsymbol{\xi}} = 0 \tag{7}$$

Using divergence theorem three times, we obtain the BIE for $u_{p,k}(\mathbf{x})$:

$$\begin{aligned} -Cu_{p,k}(\mathbf{x}) = &\int_{\partial\Omega} t_j(\xi)u_{j,k}^{*p}(\mathbf{x},\boldsymbol{\xi})dS_{\boldsymbol{\xi}} + \int_{\partial\Omega} D(\boldsymbol{\xi})u_m(\boldsymbol{\xi})e_{nk}\sigma_{nm}^{*p}(\mathbf{x},\boldsymbol{\xi})dS_{\boldsymbol{\xi}} \\ &+ \int_\Omega \bar{f}_j(\boldsymbol{\xi})u_{j,k}^{*p}(\mathbf{x},\boldsymbol{\xi})d\Omega_{\boldsymbol{\xi}} \end{aligned} \tag{8}$$

where the tangential differential operator D is:

$$\begin{aligned} D(\boldsymbol{\xi}) &= n_r(\boldsymbol{\xi})\, e_{rs} \frac{\partial}{\partial \xi_s} \\ D(\mathbf{x}) &= n_r(\mathbf{x})\, e_{rs} \frac{\partial}{\partial x_s} \end{aligned} \tag{9}$$

Eq. (8) was originally given in [Okada, Rajiyah, and Atluri (1988,1989)]. The integral representation in (8) is only strongly-singular, as opposed to the hyper-singular BIE for displacement gradients, obtained by directly differentiating Eq.(5). Pre-multiplying (8) by $n_a(\mathbf{x})E_{abpk}$, and using the inherent property of Kelvin's solution, we obtain the *(only strongly-singular, and not hyper-singular)* traction BIE of 2D plane elasticity:

$$\begin{aligned} -Ct_b(\mathbf{x}) = &\int_{\partial\Omega} t_p(\boldsymbol{\xi}) n_a(\mathbf{x}) \sigma^{*p}_{ab}(\mathbf{x},\boldsymbol{\xi}) dS_{\boldsymbol{\xi}} + \int_{\partial\Omega} D(\boldsymbol{\xi}) u_q(\xi) n_a(\mathbf{x}) \Sigma^{*}_{abq}(\mathbf{x},\boldsymbol{\xi}) dS_{\boldsymbol{\xi}} \\ &+ \int_{\Omega} \bar{f}_p(\boldsymbol{\xi}) n_a(\mathbf{x}) \sigma^{*p}_{ab}(\mathbf{x},\boldsymbol{\xi}) d\Omega_{\boldsymbol{\xi}} \end{aligned} \tag{10}$$

where

$$\Sigma^{*}_{abq}(\mathbf{x},\boldsymbol{\xi}) = E_{abkl} e_{nl} \sigma^{*k}_{nq}(\mathbf{x},\boldsymbol{\xi}) \tag{11}$$

According to the Helmholtz theorem, any vector field (and of course, second order tensor, third order tensor, etc.) can be decomposed into the summation of an irrotational field and a solenoidal field. Therefore, $\sigma^{*p}_{ij}(\mathbf{x},\boldsymbol{\xi})$ can be decomposed as:

$$\sigma^{*p}_{ij}(\mathbf{x},\boldsymbol{\xi}) = -\phi^{*p}_{ij}(\mathbf{x},\boldsymbol{\xi}) + \psi^{*p}_{ij}(\mathbf{x},\xi) \tag{12}$$

where

$$\begin{aligned} \phi^{*p}_{ij}(\mathbf{x},\boldsymbol{\xi}) &= M^{*p}_{j,i}(\mathbf{x},\boldsymbol{\xi}) \\ \psi^{*p}_{ij}(\mathbf{x},\boldsymbol{\xi}) &= e_{is} G^{*p}_{j,s}(\mathbf{x},\boldsymbol{\xi}) \end{aligned} \tag{13}$$

And $\Sigma^{*}_{ijq}(\mathbf{x},\boldsymbol{\xi})$ can be decomposed as:

$$\Sigma^{*}_{ijq}(\mathbf{x},\boldsymbol{\xi}) = -\Lambda^{*}_{ijq}(\mathbf{x},\boldsymbol{\xi}) + K^{*}_{ijq}(\mathbf{x},\boldsymbol{\xi}) \tag{14}$$

where

$$\begin{aligned} \Lambda^{*}_{ijq}(\mathbf{x},\boldsymbol{\xi}) &= N^{*}_{jq,i}(\mathbf{x},\boldsymbol{\xi}) \\ K^{*}_{ijq}(\mathbf{x},\boldsymbol{\xi}) &= e_{is} H^{*}_{jq,s}(\mathbf{x},\boldsymbol{\xi}) \end{aligned} \tag{15}$$

It is well known that the 2D fundamental solution and its corresponding displacement-gradient and stress fields are:

$$
\begin{aligned}
u_j^{*p} &= \frac{1}{8\pi\mu(1-\bar{\nu})}\left[-(3-4\bar{\nu})\ln r\delta_{jp}+r_{,j}r_{,p}\right] \\
u_{j,k}^{*p} &= \frac{1}{8\pi\mu(1-\bar{\nu})r}\left[-(3-4\bar{\nu})r_{,k}\delta_{jp}-2r_{,j}r_{,p}r_{,k}+\delta_{pk}r_{,j}+\delta_{jk}r_{,p}\right] \\
\sigma_{ij}^{*p} &= \frac{1}{4\pi(1-\bar{\nu})r}\left[(1-2\bar{\nu})(\delta_{ij}r_{,p}-\delta_{ip}r_{,j}-\delta_{jp}r_{,i})-2r_{,i}r_{,j}r_{,p}\right] \\
\Sigma_{ijq}^{*} &= \frac{\mu}{2\pi(1-\bar{\nu})r}e_{in}\left[2r_{,j}r_{,q}r_{,n}+\delta_{qj}r_{,n}-\delta_{qn}r_{,j}-\delta_{jn}r_{,q}\right]
\end{aligned}
\tag{16}
$$

Therefore, the decomposition of $\sigma_{ij}^{*p}(\mathbf{x},\xi)$ and $\Sigma_{ijq}^{*}(\mathbf{x},\boldsymbol{\xi})$can be worked out in detail in the way presented in [Dong and Atluri (2013a)]:

$$
\begin{aligned}
G_j^{*p} =& \frac{1}{8\pi(1-\bar{\nu})}\left[e_{pj}\left[(4\bar{\nu}-3)+2(2\bar{\nu}-1)\ln r\right]+2e_{kj}r_{,k}r_{,p}\right] \\
\Psi_{ij}^{*p} =& e_{is}G_{j,s}^{*p} = \frac{1}{4\pi(1-\bar{\nu})r}\left[(1-2\bar{\nu})(\delta_{ij}r_{,p}-\delta_{ip}r_{,j})-2r_{,i}r_{,j}r_{,p}+\delta_{jp}r_{,i}\right] \\
M_j^{*p} =& \frac{1}{2\pi}\left(1+\ln r\right)\delta_{pj} \\
\phi_{ij}^{*p} =& M_{j,i}^{*p} = \frac{1}{2\pi r}\delta_{pj}r_{,i} \\
H_{jq}^{*} =& \frac{\mu}{4\pi(1-\bar{\nu})}\left[\delta_{qj}\left(3+2\ln r\right)-2r_{,j}r_{,q}\right]
\end{aligned}
\tag{17}
$$

As shown in [Han and Atluri (2003)], the decomposed kernel functions can be used to regularize the displacement and traction BIEs. Using the same approach, we consider the traction BIE (10) and a test function $w_b(\mathbf{x})$, and write down the Petrov-Galerkin weak-form:

$$
\begin{aligned}
-\frac{1}{2}\int_{\partial\Omega} w_b(\mathbf{x})t_b(\mathbf{x})dS_{\mathbf{x}} = & \int_{\partial\Omega} w_b(\mathbf{x})dS_{\mathbf{x}}\int_{\partial\Omega} t_q(\boldsymbol{\xi})n_a(\mathbf{x})\sigma_{ab}^{*q}(\mathbf{x},\boldsymbol{\xi})\,dS_{\boldsymbol{\xi}} \\
& + \int_{\partial\Omega} w_b(\mathbf{x})dS_{\mathbf{x}}\int_{\partial\Omega} D(\boldsymbol{\xi})u_q(\boldsymbol{\xi})n_a(\mathbf{x})\Sigma_{abq}^{*}(\mathbf{x},\boldsymbol{\xi})dS_{\boldsymbol{\xi}} \\
& + \int_{\partial\Omega} w_b(\mathbf{x})dS_{\mathbf{x}}\int_{\Omega} \bar{f}_q(\boldsymbol{\xi})n_a(\mathbf{x})\sigma_{ab}^{*q}(\mathbf{x},\boldsymbol{\xi})\,d\Omega_{\boldsymbol{\xi}}
\end{aligned}
\tag{18}
$$

Similarly, using the displacement BIE in (5), and using a test function $v_b(\mathbf{x})$, we

write down the Petrov-Galerkin weak-form:

$$\begin{aligned}\frac{1}{2}\int_{\partial\Omega} v_p(\mathbf{x})u_p(\mathbf{x})dS_x = &\int_{\partial\Omega} v_p(\mathbf{x})dS_x \int_{\partial\Omega} t_j(\boldsymbol{\xi})u_j^{*p}(\mathbf{x},\boldsymbol{\xi})dS_{\boldsymbol{\xi}} \\ &- \int_{\partial\Omega} v_p(\mathbf{x})dS_x \int_{\partial\Omega} n_i(\boldsymbol{\xi})u_j(\boldsymbol{\xi})\sigma_{ij}^{*p}(\mathbf{x},\boldsymbol{\xi})\,dS_{\boldsymbol{\xi}} \\ &+ \int_{\partial\Omega} v_p(\mathbf{x})dS_x \int_{\partial\Omega} \bar{f}_j(\boldsymbol{\xi})u_j^{*p}(\mathbf{x},\boldsymbol{\xi})d\Omega_{\boldsymbol{\xi}}\end{aligned} \tag{19}$$

Substituting (12)-(15) into (18) and (19), and integrating by parts, we have:

$$\begin{aligned}&\frac{1}{2}\int_{\partial\Omega} v_p(\mathbf{x})u_p(\mathbf{x})dS_x \\ &= \int_{\partial\Omega} v_p(\mathbf{x})dS_x \int_{\partial\Omega} t_j(\boldsymbol{\xi})u_j^{*p}(\mathbf{x},\boldsymbol{\xi})dS_{\boldsymbol{\xi}} \\ &+ \int_{\partial\Omega} v_p(\mathbf{x})dS_x \int_{\partial\Omega} D(\boldsymbol{\xi})u_j(\boldsymbol{\xi})G_j^{*p}(\mathbf{x},\boldsymbol{\xi})\,dS_{\boldsymbol{\xi}} \\ &+ \int_{\partial\Omega} v_p(\mathbf{x})dS_x \int_{\partial\Omega} n_i(\boldsymbol{\xi})u_j(\boldsymbol{\xi})\phi_{ij}^{*p}(\mathbf{x},\boldsymbol{\xi})\,dS_{\boldsymbol{\xi}} \\ &+ \int_{\partial\Omega} v_p(\mathbf{x})dS_x \int_{\partial\Omega} \bar{f}_j(\boldsymbol{\xi})u_j^{*p}(\mathbf{x},\boldsymbol{\xi})d\Omega_{\boldsymbol{\xi}}\end{aligned} \tag{20}$$

$$\begin{aligned}&-\frac{1}{2}\int_{\partial\Omega} w_b(\mathbf{x})t_b(\mathbf{x})dS_{\mathbf{x}} \\ &= \int_{\partial\Omega} D(\mathbf{x})w_b(\mathbf{x})dS_{\mathbf{x}} \int_{\partial\Omega} t_q(\boldsymbol{\xi})G_b^{*q}(\mathbf{x},\boldsymbol{\xi})\,dS_{\boldsymbol{\xi}} \\ &- \int_{\partial\Omega} w_b(\mathbf{x})dS_{\mathbf{x}} \int_{\partial\Omega} n_a(\mathbf{x})t_q(\boldsymbol{\xi})\phi_{ab}^{*q}(\mathbf{x},\boldsymbol{\xi})\,dS_{\boldsymbol{\xi}} \\ &+ \int_{\partial\Omega} D(\mathbf{x})w_b(\mathbf{x})dS_{\mathbf{x}} \int_{\partial\Omega} D(\boldsymbol{\xi})u_q(\boldsymbol{\xi})H_{bq}^{*}(\mathbf{x},\boldsymbol{\xi})dS_{\boldsymbol{\xi}} \\ &+ \int_{\partial\Omega} w_b(\mathbf{x})dS_{\mathbf{x}} \int_{\Omega} \bar{f}_q(\boldsymbol{\xi})n_a(\mathbf{x})\sigma_{ab}^{*q}(\mathbf{x},\boldsymbol{\xi})\,d\Omega_{\boldsymbol{\xi}}\end{aligned} \tag{21}$$

When $w_b = \delta u_b$, $v_b = \delta t_b$ is used, equations (20)(21) leads to Symmetric Galerkin BIEs and global SGBEMs. The current BIEs are different from a lot of previous SGBEM studies which involve regularization of hyper-singular kernels, such as [Frangi and Novati (1996); Bonnet, Maier and Polizzotto (1998); Li, Mear and Xiao (1998); Frangi, Novati, Springhetti, Rovizzi (2002)]. Eq. (20)(21) developed here are only weakly singular, because the kernels $u_b^{*q}(\mathbf{x},\boldsymbol{\xi})$, $G_b^{*q}(\mathbf{x},\boldsymbol{\xi})$, $H_{bq}^{*}(\mathbf{x},\boldsymbol{\xi})$, $n_i(\boldsymbol{\xi})\phi_{ij}^{*p}(\mathbf{x},\boldsymbol{\xi})$, $n_i(\mathbf{x})\phi_{ij}^{*p}(\mathbf{x},\boldsymbol{\xi})$ are all weakly-singular. Therefore, the implementation of (21)(20) for SGBEM can be carried out much more easily.

It should also be pointed out that,the Symmetric Galerkin BIEs for 2D problems as shown here, are only slightly different from the BIEs presented in [Han and Atluri

(2003)]. For example, the tensors $\mathbf{G}^*, \mathbf{H}^*, \mathbf{\Sigma}^*$ have different orders. We would like to point out that, this slight difference originates from the difference between the 2D Levi-Civita symbol e_{rs} and the 3D Levi-Civitasymbol e_{rst}. In other words, the difference arises because of the fact that the curl of a vector field, and the cross-product of two in-plane vectors, are out-of-plane. If one carefully distinguishes the in-plane and out-of-plane components of each tensor and vector in [Han and Atluri (2003)], one can see that BIEs developed in [Han and Atluri (2003)] are equivalent to the current ones. However, in this study, we keep the present way, for clarity.

3 SGBEM Voronoi Cell (SVC) with Arbitrary Voids and Inclusions

In this Section, we apply the BIEs developed in section 2, to a local polygonal subdomain Ω containing arbitrary shaped voids and elastic/rigid inclusions, and develop a Voronoi Cell (SVC), with its own stiffness matrix, by using some algebraic manipulations. We first consider that the subdomain Ω is homogenous and isotropic, but it can contain arbitrarily-shaped voids in it, as in Fig. 2, or arbitrarily shaped inclusions which can be of a different material. Without distinguishing what types of boundary conditions are considered at $\partial\Omega$, we assume the boundary displacements as $u_i = \mathbf{N}\mathbf{q}_i$ and boundary tractions as $t_i = \mathbf{M}\mathbf{p}_i$, both at the entire boundary $\partial\Omega$ of the local subdomain. By using both the displacement BIE (20) and traction BIE (21) for the entire $\partial\Omega$, we have:

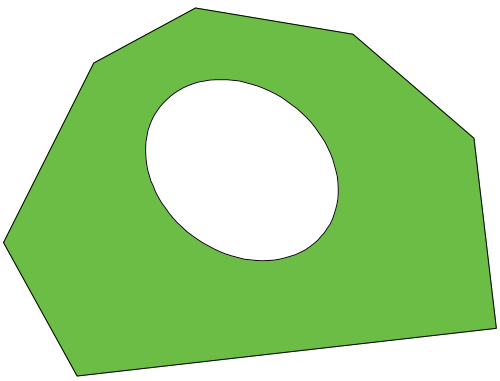

Figure 2: An SGBEM Voronoi Cell (SVC) with a Void

$$\begin{array}{l} -\frac{1}{2}\delta\mathbf{p}_j^T \int_{\partial\Omega}\mathbf{M}^T(\mathbf{x})\mathbf{N}(\mathbf{x})dS_x\mathbf{q}_j \\ = -\delta\mathbf{p}_p^T \int_{\partial\Omega}\mathbf{M}^T(\mathbf{x})dS_x \int_{\partial\Omega} u_j^{*p}(\mathbf{x},\boldsymbol{\xi})\mathbf{M}(\boldsymbol{\xi})dS_{\boldsymbol{\xi}}\mathbf{p}_j \\ -\delta\mathbf{p}_p^T \int_{\partial\Omega}\mathbf{M}^T(\mathbf{x})dS_x \int_{\partial\Omega} G_j^{*p}(\mathbf{x},\boldsymbol{\xi})D(\boldsymbol{\xi})\mathbf{N}(\xi)dS_{\boldsymbol{\xi}}\mathbf{q}_j \\ -\delta\mathbf{p}_p^T \int_{\partial\Omega}\mathbf{M}^T(\mathbf{x})dS_x \int_{\partial\Omega} n_i(\xi)\phi_{ij}^{*p}(\mathbf{x},\boldsymbol{\xi})\mathbf{N}(\xi)dS_{\boldsymbol{\xi}}\mathbf{q}_j \end{array} \tag{22}$$

$$\begin{array}{l} \frac{1}{2}\delta\mathbf{q}_b^T \int_{\partial\Omega}\mathbf{N}(\mathbf{x})^T\mathbf{M}(\mathbf{x})dS_{\mathbf{x}}\mathbf{p}_b \\ = -\delta\mathbf{q}_b^T \int_{\partial\Omega} D(\mathbf{x})\mathbf{N}^T(\mathbf{x})dS_{\mathbf{x}} \int_{\partial\Omega} G_b^{*q}(\mathbf{x},\boldsymbol{\xi})\mathbf{M}(\xi)dS_{\boldsymbol{\xi}}\mathbf{p}_q \\ +\delta\mathbf{q}_b^T \int_{\partial\Omega}\mathbf{N}(\mathbf{x})^T dS_{\mathbf{x}} \int_{\partial\Omega} n_a(\mathbf{x})\phi_{ab}^{*q}(\mathbf{x},\boldsymbol{\xi})\mathbf{M}(\boldsymbol{\xi})dS_{\boldsymbol{\xi}}\mathbf{p}_q \\ -\delta\mathbf{q}_b^T \int_{\partial\Omega} D(\mathbf{x})\mathbf{N}^T(\mathbf{x})dS_{\mathbf{x}} \int_{\partial\Omega} H_{bq}^*(\mathbf{x},\boldsymbol{\xi})D(\xi)\mathbf{N}(\boldsymbol{\xi})dS_{\boldsymbol{\xi}}\mathbf{q}_q \end{array} \tag{23}$$

Without ambiguity, one can rewrite (22)(23) as:

$$-\frac{1}{2}\delta\mathbf{p}^T\mathbf{U}\mathbf{q} = \delta\mathbf{p}^T\mathbf{P}\mathbf{P}\mathbf{p} + \delta\mathbf{p}^T\mathbf{P}\mathbf{Q}\mathbf{q} \tag{24}$$

$$\frac{1}{2}\delta\mathbf{q}^T\mathbf{T}\mathbf{p} = \delta\mathbf{q}^T\mathbf{Q}\mathbf{P}\mathbf{p} + \delta\mathbf{q}^T\mathbf{Q}\mathbf{Q}\mathbf{q} \tag{25}$$

where(24) corresponds to (22), and (25) corresponds to (23).

From the property of SGBEM, or by some trivial math manipulation, one can see that, if $\mathbf{M} = \mathbf{N}$, then:

$$\begin{array}{l} \mathbf{U} = \mathbf{T}^T \\ \mathbf{P}\mathbf{P} = \mathbf{P}\mathbf{P}^T \\ \mathbf{Q}\mathbf{Q} = \mathbf{Q}\mathbf{Q}^T \\ \mathbf{P}\mathbf{Q} = \mathbf{Q}\mathbf{P}^T \end{array} \tag{26}$$

One can easily rewrite (24)(25) as:

$$\mathbf{0} = \delta\mathbf{p}^T\mathbf{P}\mathbf{P}\mathbf{p} + \delta\mathbf{p}^T\left(\mathbf{P}\mathbf{Q} + \frac{1}{2}\mathbf{U}\right)\mathbf{q} \tag{27}$$

$$\delta\mathbf{q}^T\mathbf{T}\mathbf{p} = \delta\mathbf{q}^T\left(\mathbf{Q}\mathbf{P} + \frac{1}{2}\mathbf{T}\right)\mathbf{p} + \delta\mathbf{q}^T\mathbf{Q}\mathbf{Q}\mathbf{q} \tag{28}$$

Because $\delta\mathbf{p}$ is arbitrary (unlike $\delta\mathbf{q}$), we can use static condensation of (27)(28) to obtain:

$$\delta\mathbf{q}^T\mathbf{T}\mathbf{p} = \delta\mathbf{q}^T\left[\mathbf{Q}\mathbf{Q} - \left(\mathbf{Q}\mathbf{P} + \frac{1}{2}\mathbf{T}\right)\mathbf{P}\mathbf{P}^{-1}\left(\mathbf{P}\mathbf{Q} + \frac{1}{2}\mathbf{U}\right)\right]\mathbf{q} \tag{29}$$

From the properties in (26), we can see that the matrix in the right-hand side is symmetric.

One more interesting observation is that:

$$\begin{aligned}\delta\mathbf{q}^T\mathbf{T}\mathbf{p} &= \delta\mathbf{q}_b^T\int_{\partial\Omega}\mathbf{N}(\mathbf{x})^T\mathbf{M}(\mathbf{x})dS_{\mathbf{x}}\mathbf{p}_b \\ &= \delta\mathbf{q}_b^T\int_{\partial\Omega}\mathbf{N}(\mathbf{x})^{\mathbf{T}}\mathbf{t}_{\mathbf{b}}(\mathbf{x})dS_{\mathbf{x}} \\ &= \delta\mathbf{q}^T\mathbf{Q}\end{aligned} \tag{30}$$

where the vector $\mathbf{Q}$ has the exact form of the generalized "force vector" as in FEM. Therefore, it is clear that the right hand side of (29) has the physical meaning of the variation of strain-energy of Ω, and the symmetric matrix can be considered as the "stiffness matrix" of the local subdomain Ω. Eq.(29) can be therefore written as:

$$\delta\mathbf{q}^T\mathbf{Q} = \delta\mathbf{q}^T\mathbf{K}\mathbf{q} \tag{31}$$

For numerical implementation, one can simply evaluate the stiffness matrix of the SVC, as:

$$\mathbf{K} = \mathbf{Q}\mathbf{Q} - \left(\mathbf{Q}\mathbf{P} + \frac{1}{2}\mathbf{T}\right)\mathbf{P}\mathbf{P}^{-1}\left(\mathbf{P}\mathbf{Q} + \frac{1}{2}\mathbf{U}\right) \tag{32}$$

One can also evaluate the force vector $\mathbf{Q}$ using the usual FEM procedure.

One direct result of the assembly of different SVCs is a microstructurewith inclusions. One can first develop the stiffness matrix of a SVC with holes only, and then develop a different SVC to represent an elastic or rigid inclusion, with exactly the same shape as that of the hole, but with a different material, as shown in Fig. 3. By assembling these two SVCs together, one obtains an SVC with elastic or rigid inclusions. Without loss of generality, we consider an SVC with only one inclusion. We use $\mathbf{q_m}, \mathbf{q_c}$ to denote the degree of freedoms on the outer boundary of the parent SVC, and at the matrix-inclusion interface. The FEM equation of the matrix material can be developed as:

$$\begin{Bmatrix}\delta\mathbf{q_m}\\ \delta\mathbf{q_c}\end{Bmatrix}^{\mathbf{T}}\begin{bmatrix}\mathbf{K_{mm}} & \mathbf{K_{mc}}\\ \mathbf{K_{cm}} & \mathbf{K_{cc}}\end{bmatrix}\begin{Bmatrix}\mathbf{q_m}\\ \mathbf{q_c}\end{Bmatrix} = \begin{Bmatrix}\delta\mathbf{q_m}\\ \delta\mathbf{q_c}\end{Bmatrix}^{\mathbf{T}}\begin{Bmatrix}\mathbf{Q_m}\\ \mathbf{Q_c}\end{Bmatrix} \tag{33}$$

If no external force is applied at the matrix-inclusion interface, the FEM equation of the inclusion can be written as:

$$\delta\mathbf{q_c}^{\mathbf{T}}\bar{\mathbf{K}}_{\mathbf{cc}}\mathbf{q_c} = -\delta\mathbf{q_c}^{\mathbf{T}}\mathbf{Q_c} \tag{34}$$

By using the assembly procedure, the FEM equations of the SVC with an inclusion can be written as:

$$\begin{Bmatrix}\delta\mathbf{q_m}\\ \delta\mathbf{q_c}\end{Bmatrix}^{\mathbf{T}}\begin{bmatrix}\mathbf{K_{mm}} & \mathbf{K_{mc}}\\ \mathbf{K_{cm}} & \mathbf{K_{cc}}+\bar{\mathbf{K}}_{\mathbf{cc}}\end{bmatrix}\begin{Bmatrix}\mathbf{q_m}\\ \mathbf{q_c}\end{Bmatrix} = \begin{Bmatrix}\delta\mathbf{q_m}\\ \delta\mathbf{q_c}\end{Bmatrix}^{\mathbf{T}}\begin{Bmatrix}\mathbf{Q_m}\\ \mathbf{0}\end{Bmatrix} \tag{35}$$

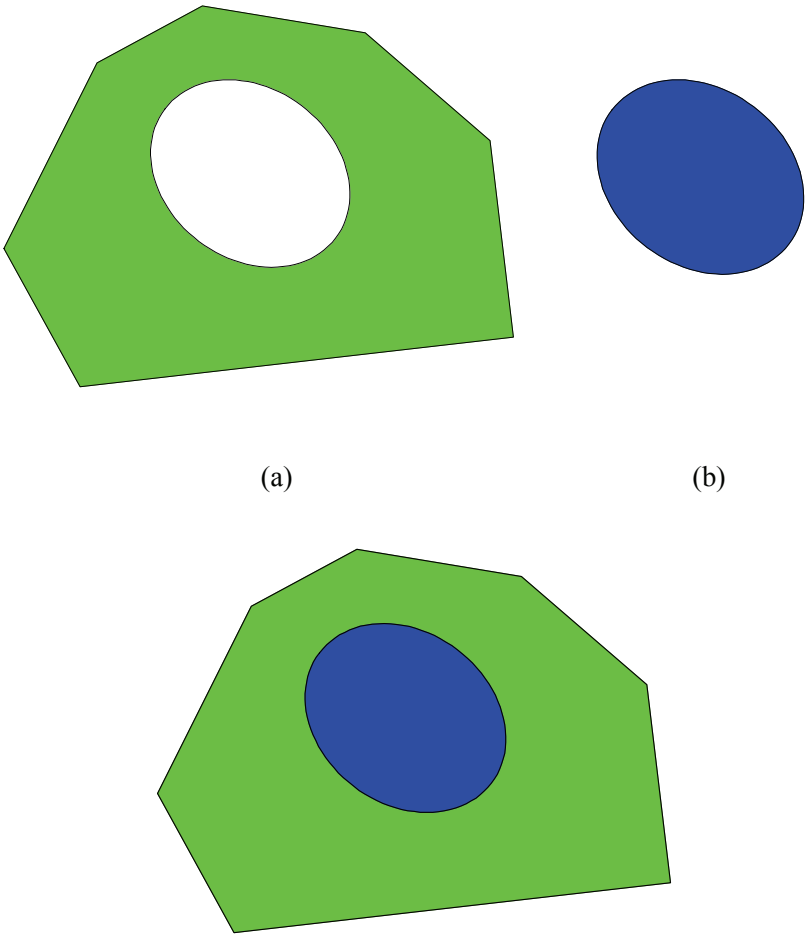

Figure 3: (a) SVC for the matrix material; (b) SVC for the inclusion material, which can be different from the matrix material; (c)the assembled SVC with an inclusion

Using static condensation (35) can be rewritten as:

$$\delta \mathbf{q}_m^{\mathbf{T}} \bar{\mathbf{K}}_{mm} \mathbf{q}_m = \delta \mathbf{q}_m^{\mathbf{T}} \mathbf{Q}_m \tag{36}$$

where

$$\bar{\mathbf{K}}_{\mathbf{mm}} = \mathbf{K}_{\mathbf{mm}} - \mathbf{K}_{\mathbf{mc}} \left(\mathbf{K}_{\mathbf{cc}} + \bar{\mathbf{K}}_{\mathbf{cc}} \right)^{-1} \mathbf{K}_{\mathbf{cm}} \tag{37}$$

It should be noted that, the SVCs developed in this study do not involve Lagrange multipliers at all. Therefore, no L.B.B. conditions as in [Brezzi (1974)] are involved, which plagues the stability of solution by hybrid/mixed FEMs

4 SVC with ArbitraryShaped Micro-Cracks

The SVC developed in last section is for a grain of a material without any micro-cracks. However, when micro-cracks are present, some modifications are necessary. This is because of the fact that, the weakly-singular BIEs developed in section 2, can only allow users to consider cracks as part of the traction-prescribed boundary, where unkowns are the displacement discontinuity Δu_i at crack surface S_c. Therefore,the traction BIE(21), in a symmetric Galerkin weak form, can be directly applied to the crack surface. On the other hand, the displacement BIE (20) as developed in section 2 cannot be directly applied to crack surfaces.

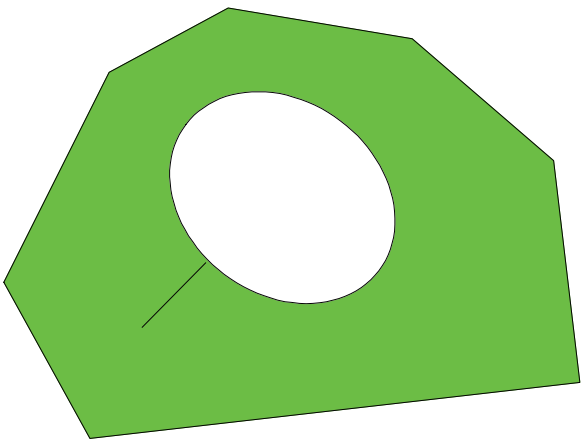

Figure 4: An SVC (a grain of a material) with a Void and a Micro-crack

Therefore, the following modifications are made. Consider the boundary of domain Ω which can be divided into S_b and S_c, where S_b is the summation of all the close contours representing the outer boundary and the inner cavities, and S_c is the summation of crack surfaces, see Fig. 4. We assume both the unknown displacements $u_i = \mathbf{N}\mathbf{q}_i$ and the tractions $t_i = \mathbf{M}\mathbf{p}_i$ at the entireboundary S_b, and we only assume displacement jumps at the crack surface S_c as $\Delta u_i = \mathbf{L}\mathbf{r}_i$. Then we write down the following equations:

$$\begin{array}{l} -\frac{1}{2}\delta\mathbf{p}_j^T \int_{S_b} \mathbf{M}^T(\mathbf{x})\mathbf{N}(\mathbf{x})dS_x\mathbf{q}_j \\ = -\delta\mathbf{p}_p^T \int_{S_b} \mathbf{M}^T(\mathbf{x})dS_x \int_{S_b} u_j^{*p}(\mathbf{x},\boldsymbol{\xi})\mathbf{M}(\boldsymbol{\xi})dS_{\boldsymbol{\xi}}\mathbf{p}_j \\ -\delta\mathbf{p}_p^T \int_{S_b} \mathbf{M}^T(\mathbf{x})dS_x \int_{S_b} G_j^{*p}(\mathbf{x},\boldsymbol{\xi})D(\xi)\mathbf{N}(\boldsymbol{\xi})dS_{\boldsymbol{\xi}}\mathbf{q}_j \\ -\delta\mathbf{p}_p^T \int_{S_b} \mathbf{M}^T(\mathbf{x})dS_x \int_{S_b} n_i(\boldsymbol{\xi})\phi_{ij}^{*p}(\mathbf{x},\boldsymbol{\xi})\mathbf{N}(\boldsymbol{\xi})dS_{\boldsymbol{\xi}}\mathbf{q}_j \\ -\delta\mathbf{p}_p^T \int_{S_b} \mathbf{M}^T(\mathbf{x})dS_x \int_{S_c} G_j^{*p}(\mathbf{x},\boldsymbol{\xi})D(\xi)\mathbf{L}(\boldsymbol{\xi})dS_{\boldsymbol{\xi}}\mathbf{r}_j \\ -\delta\mathbf{p}_p^T \int_{S_b} \mathbf{M}^T(\mathbf{x})dS_x \int_{S_c} n_i(\boldsymbol{\xi})\phi_{ij}^{*p}(\mathbf{x},\boldsymbol{\xi})\mathbf{L}(\boldsymbol{\xi})dS_{\boldsymbol{\xi}}\mathbf{r}_j \end{array} \tag{38}$$

$$\begin{array}{l} \frac{1}{2}\delta\mathbf{q}_b^T \int_{S_b} \mathbf{N}(\mathbf{x})^T\mathbf{M}(\mathbf{x})dS_{\mathbf{x}}\mathbf{p}_b \\ = -\delta\mathbf{q}_b^T \int_{S_b} D(\mathbf{x})\mathbf{N}^T(\mathbf{x})dS_{\mathbf{x}} \int_{S_b} G_b^{*q}(\mathbf{x},\boldsymbol{\xi})\mathbf{M}(\boldsymbol{\xi})dS_{\boldsymbol{\xi}}\mathbf{p}_q \\ +\delta\mathbf{q}_b^T \int_{S_b} \mathbf{N}(\mathbf{x})^T dS_{\mathbf{x}} \int_{S_b} n_a(\mathbf{x})\phi_{ab}^{*q}(\mathbf{x},\boldsymbol{\xi})\mathbf{M}(\boldsymbol{\xi})dS_{\boldsymbol{\xi}}\mathbf{p}_q \\ -\delta\mathbf{q}_b^T \int_{S_b} D(\mathbf{x})\mathbf{N}^T(\mathbf{x})dS_{\mathbf{x}} \int_{S_b} H_{bq}^*(\mathbf{x},\boldsymbol{\xi})D(\boldsymbol{\xi})\mathbf{N}(\boldsymbol{\xi})dS_{\boldsymbol{\xi}}\mathbf{q}_q \\ -\delta\mathbf{q}_b^T \int_{S_b} D(\mathbf{x})\mathbf{N}^T(\mathbf{x})dS_{\mathbf{x}} \int_{S_c} H_{bq}^*(\mathbf{x},\boldsymbol{\xi})D(\boldsymbol{\xi})\mathbf{L}(\boldsymbol{\xi})dS_{\boldsymbol{\xi}}\mathbf{r}_q \end{array} \tag{39}$$

$$\begin{array}{l} \delta\mathbf{r}_b^T \int_{S_c} \mathbf{L}(\mathbf{x})^T\bar{t}_b(\mathbf{x})dS_{\mathbf{x}} \\ = -\delta\mathbf{r}_b^T \int_{S_c} D(\mathbf{x})\mathbf{L}^T(\mathbf{x})dS_{\mathbf{x}} \int_{S_b} G_b^{*q}(\mathbf{x},\boldsymbol{\xi})\mathbf{M}(\boldsymbol{\xi})dS_{\boldsymbol{\xi}}\mathbf{p}_q \\ +\delta\mathbf{r}_b^T \int_{S_c} \mathbf{L}(\mathbf{x})^T dS_{\mathbf{x}} \int_{S_b} n_a(\mathbf{x})\phi_{ab}^{*q}(\mathbf{x},\boldsymbol{\xi})\mathbf{M}(\boldsymbol{\xi})dS_{\boldsymbol{\xi}}\mathbf{p}_q \\ -\delta\mathbf{r}_b^T \int_{S_c} D(\mathbf{x})\mathbf{L}^T(\mathbf{x})dS_{\mathbf{x}} \int_{S_b} H_{bq}^*(\mathbf{x},\boldsymbol{\xi})D(\boldsymbol{\xi})\mathbf{N}(\boldsymbol{\xi})dS_{\boldsymbol{\xi}}\mathbf{q}_q \\ -\delta\mathbf{r}_b^T \int_{S_c} D(\mathbf{x})\mathbf{L}^T(\mathbf{x})dS_{\mathbf{x}} \int_{S_c} H_{bq}^*(\mathbf{x},\boldsymbol{\xi})D(\boldsymbol{\xi})\mathbf{L}(\boldsymbol{\xi})dS_{\boldsymbol{\xi}}\mathbf{r}_q \end{array} \tag{40}$$

Without ambiguity, one can rewrite these equations as:

$$-\frac{\mathbf{1}}{\mathbf{2}}\boldsymbol{\delta}\mathbf{p}^{\mathbf{T}}\mathbf{U}\mathbf{q} = \boldsymbol{\delta}\mathbf{p}^{\mathbf{T}}\mathbf{P}\mathbf{P}\mathbf{p} + \boldsymbol{\delta}\mathbf{p}^{\mathbf{T}}\mathbf{P}\mathbf{Q}\mathbf{q} + \boldsymbol{\delta}\mathbf{p}^{\mathbf{T}}\mathbf{P}\mathbf{R}\mathbf{r} \tag{41}$$

$$\frac{1}{2}\delta\mathbf{q}^T\mathbf{T}\mathbf{p} = \delta\mathbf{q}^T\mathbf{Q}\mathbf{P}\mathbf{p} + \delta\mathbf{q}^T\mathbf{Q}\mathbf{Q}\mathbf{q} + \delta\mathbf{q}^T\mathbf{Q}\mathbf{R}\mathbf{r} \tag{42}$$

$$\delta\mathbf{r}^T\mathbf{R} = \delta\mathbf{r}^T\mathbf{R}\mathbf{P}\mathbf{p} + \delta\mathbf{r}^T\mathbf{R}\mathbf{Q}\mathbf{q} + \delta\mathbf{r}^T\mathbf{R}\mathbf{R}\mathbf{r} \tag{43}$$

One can rewrite these equations as:

$$\mathbf{0} = \delta\mathbf{p}^T\mathbf{P}\mathbf{P}\mathbf{p} + \delta\mathbf{p}^T\left(\mathbf{P}\mathbf{Q} + \frac{1}{2}\mathbf{U}\right)\mathbf{q} + \boldsymbol{\delta}\mathbf{p}^{\mathbf{T}}\mathbf{P}\mathbf{R}\mathbf{r} \tag{44}$$

$$\delta\mathbf{q}^T\mathbf{Q} = \delta\mathbf{q}^T\left(\mathbf{Q}\mathbf{P} + \frac{1}{2}\mathbf{T}\right)\mathbf{p} + \delta\mathbf{q}^T\mathbf{Q}\mathbf{Q}\mathbf{q} + \delta\mathbf{q}^T\mathbf{Q}\mathbf{R}\mathbf{r} \tag{45}$$

$$\delta \mathbf{r}^T \mathbf{R} = \delta \mathbf{r}^T \mathbf{RPp} + \delta \mathbf{r}^T \mathbf{RQq} + \delta \mathbf{r}^T \mathbf{RRr}$$

Following the same static condensation procedure, we obtain the following equations:

$$\begin{pmatrix} \delta \mathbf{q} \\ \delta \mathbf{r} \end{pmatrix}^T \begin{bmatrix} \mathbf{K_{qq}} & \mathbf{K_{qr}} \\ \mathbf{K_{rq}} & \mathbf{K_{rr}} \end{bmatrix} \begin{pmatrix} \mathbf{q} \\ \mathbf{r} \end{pmatrix} = \begin{pmatrix} \delta \mathbf{q} \\ \delta \mathbf{r} \end{pmatrix}^T \begin{pmatrix} \mathbf{Q} \\ \mathbf{R} \end{pmatrix} \tag{46}$$

where:

$$\begin{aligned} \mathbf{K_{qq}} &= \mathbf{QQ} - \left(\mathbf{QP} + \tfrac{1}{2}\mathbf{T}\right) \mathbf{PP}^{-1} \left(\mathbf{PQ} + \tfrac{1}{2}\mathbf{U}\right) \\ \mathbf{K_{qr}} &= \mathbf{QR} - \left(\mathbf{QP} + \tfrac{1}{2}\mathbf{T}\right) \mathbf{PP}^{-1} \left(\mathbf{PR}\right) \\ \mathbf{K_{rq}} &= \mathbf{RQ} - \left(\mathbf{RP}\right) \mathbf{PP}^{-1} \left(\mathbf{PQ} + \tfrac{1}{2}\mathbf{U}\right) \\ \mathbf{K_{rr}} &= \mathbf{RR} - \left(\mathbf{RP}\right) \mathbf{PP}^{-1} \left(\mathbf{PR}\right) \end{aligned} \tag{47}$$

As described before, the vector $\mathbf{Q}$ has exactly the same form of the generalized "force vector" as in FEM, and $\boldsymbol{\delta}\mathbf{q}^T\mathbf{Q}$ has the physical meaning of work done by force $\mathbf{Q}$ subjected to the displacement $\boldsymbol{\delta}\mathbf{q}$ at the boundary S_b. We can also see that $\boldsymbol{\delta}\mathbf{r}^T\mathbf{R}$ has the physical meaning of the work done by the forces $\mathbf{R}$, which represent the crack surface tractions, subjected to the crack surface opening displacement $\boldsymbol{\delta}\mathbf{r}$. If traction free conditions are considered at the crack surfaces, the vector $\mathbf{R}$ vanishes and so does $\boldsymbol{\delta}\mathbf{r}^T\mathbf{R}$.

We also point out that, if inclusions as well as cracks are considered, one can follow the same assembly procedure used in section 3.

It should be noted that, although the SVC is implemented as a two-dimensional version in this study, it can be easily extended to three-dimensional cases, with the weakly-singular BIEs developed by [Han and Atluri (2003)], and the Wachspress shape functions as used in [Bishay and Atluri(2012); Dong and Atluri(2012c,d)].

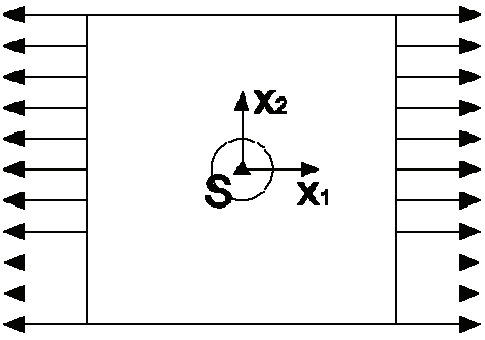

Figure 5: An infinite plate, with a circular hole/inclusion, under remote tension

5 Numerical Examples

We consider the problem of an infinite plate with a circular hole as in Fig. 5, under remote tension. The exact solution for this problem can be found in [Muskhelishvili (1954)].

Although this is actually a problem of an infinite domain, a truncated domain is used here instead. A plane stress problem with $E = 1, v = 0.25$ is considered. A 100×100 square plate is considered, and the radius of the hole is taken to be 10. Only a single SVC is used to solve this problem. The boundary discretization of the SVC has 20 nodes at the outer boundary, and 24 nodes in the cavity. The computed σ_{11} and σ_{22} are plotted along axis x_2 and x_1 respectively, in Fig. 6.

We also solve the problem of a circular inclusion. The same geometry and loading condition is considered as last example. The matrix material properties are $E_m = 1, v_m = 0.25$, and the inclusion properties are $E_c = 2, v_c = 0.3$. A single SVC with an inclusion is used to solve this problem. The boundary discretization of the SVC has 20 nodes in the outer boundary and 24 nodes in the matrix-inclusion interface. The exact solution for this problem can also be found in [Muskhelishvili (1954)]. The computed σ_{11} and σ_{22} are plotted along axis x_2 and x_1 respectively, in Fig. 7.

We consider the problem of an infinite plate with an elliptical hole as in Fig. 8 under remote tension. The exact solution for this problem can be found in [Muskhelishvili (1954)].

A 100×100 square plate is considered as the domain of interest, and the semi-axes a, b are set to be 10 and 5 respectively. A plane stress problem with $E = 1, v = 0.25$ is considered. We consider a remote tension in the x_2 direction. One SVC is used to solve this problem. The boundary discretization of the SVC has 20 nodes in the outer boundary and 36 nodes in the cavity. The computed σ_{11} and σ_{22} are plotted along axes x_2 and x_1 respectively, in Fig. 9

We also solve the problem of an elliptical inclusion. The same geometry and loading condition is considered as last example. A plane strain problem is considered. The matrix material properties are $E_m = 1, v_m = 0.25$, and the inclusion properties are $E_c = 2, v_c = 0.3$. A single SVC with an elliptical inclusion is used to solve this problem. The boundary discretization of the SVC has 20 nodes in the outer boundary and 36 nodes in the matrix-inclusion interface. The exact solution for this problem can be found by an equivalent inclusion method as in [Eshelby (1957)], considering an infinitely long cylinder. The computed σ_{11} and σ_{22} are plotted along axis x_2 and x_1 respectively, in Fig. 10.

We also consider the problem of an infinite plate with a rectangular hole under remote tension, see Fig. 11. Theoretically speaking, the exact solution of this problem requires conformal mapping which is infinite series: $z = \omega(\varsigma) = R(\frac{1}{\varsigma} + A\varsigma +$

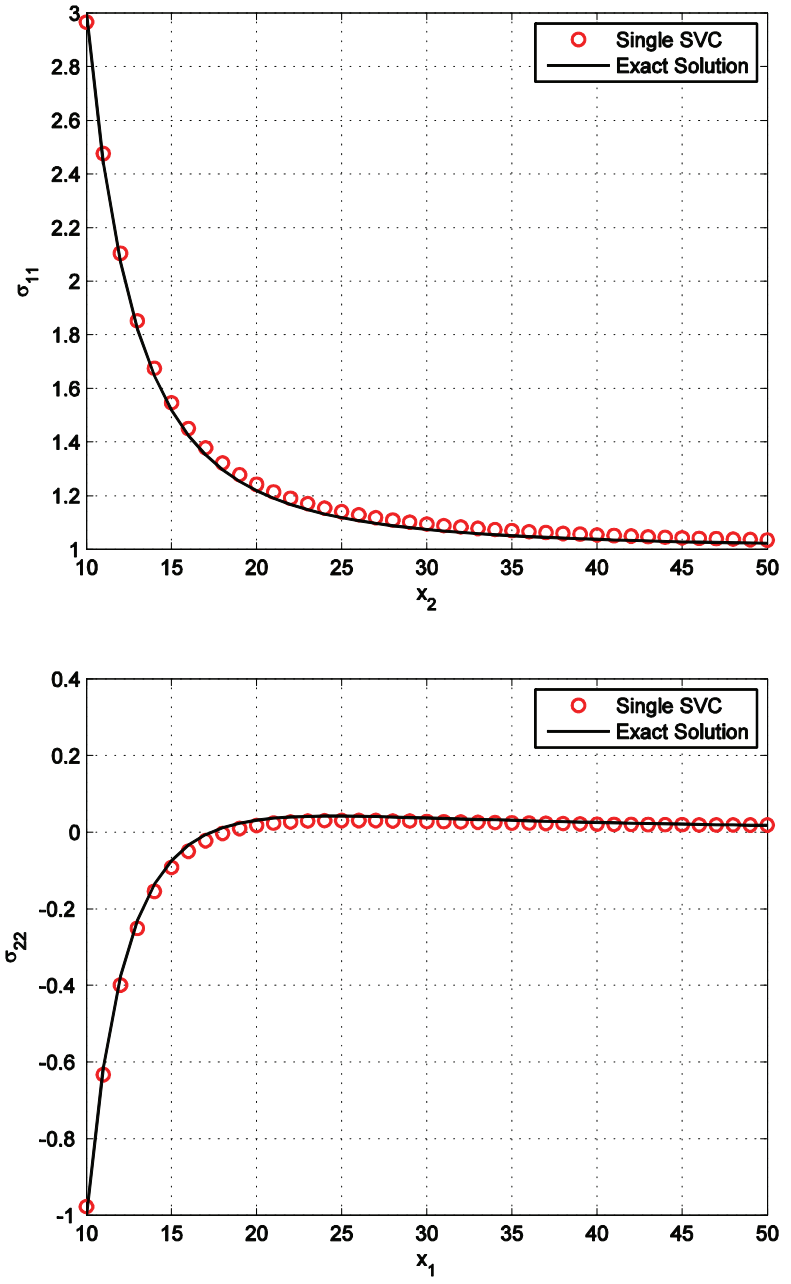

Figure 6: Computed σ_{11} along axis x_2 , and computed σ_{22} along axis x_1 for the problem of a circular hole

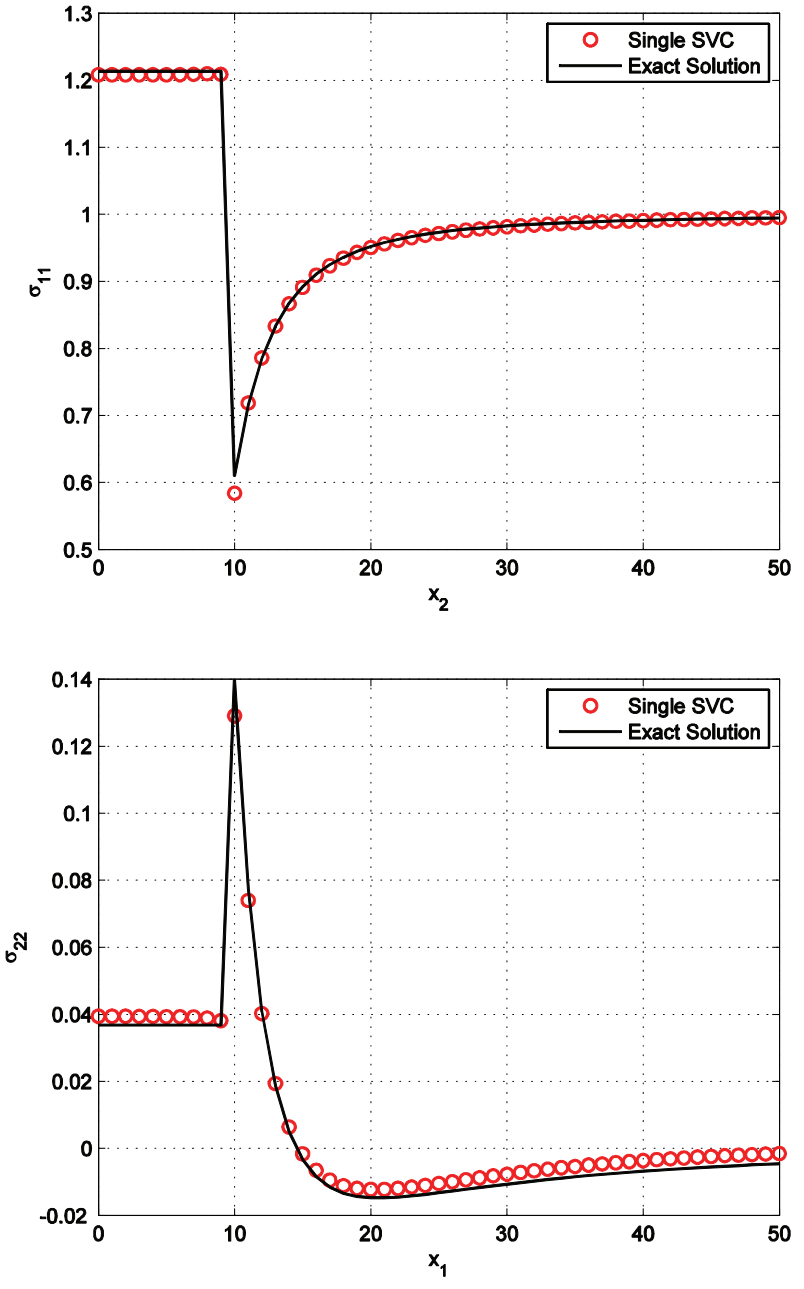

Figure 7: Computed σ_{11} along axis x_2 , and computed σ_{22} along axis x_1 for the problem of a circular inclusion

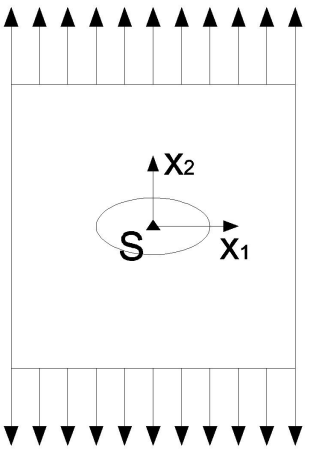

Figure 8: An infinite plate with an elliptical hole/inclusion under remote tension

$B\varsigma^3 + C\varsigma^5 + ...$), see [Savin (1961)]. However, keeping only the first four terms can produce a fairly reasonable result, as shown in [Lei, Ng, and Rigby (2001)]. In this study, we use the explicit result in [Lei, Ng, and Rigby (2001)] as the exact solution.

A 100×100 square plate is considered as the domain of interest, and both a, b are set to be 20. A single SVC is used to solve this problem. The boundary discretization of the SVC has 20 nodes in the outer boundary and 48 nodes in the cavity. The computed σ_{22} are plotted along the line AB and the line AC, in Fig. 12 and Fig. 13.

We also study the Al/SiC material by using the present SVCs. Three different volume fractions of SiC are considered: 10%, 20% and 30% of SiC respectively. For each volume fraction, an RVE with 25 polygonal SiC particles are randomly generated, as shown in Fig. 14. The material properties of Al and SiC are $E_{\mathrm{Al}} = 74GPa$, $v_{\mathrm{Al}} = 0.33$, $E_{SiC} = 410GPa$, $v_{SiC} = 0.19$. The size of the RVE is 100 μm$\times$ 100 μm. A uniform tensile stress of 100 MPa is applied in the vertical direction. The computed over-all stiffness of the composite is plotted in Fig. 15, together with results from using semi-analytical methods such as Hanshin-Strikman bounds, and the Halpin-Tsai method. As compared to the experimental results of [Chawla,

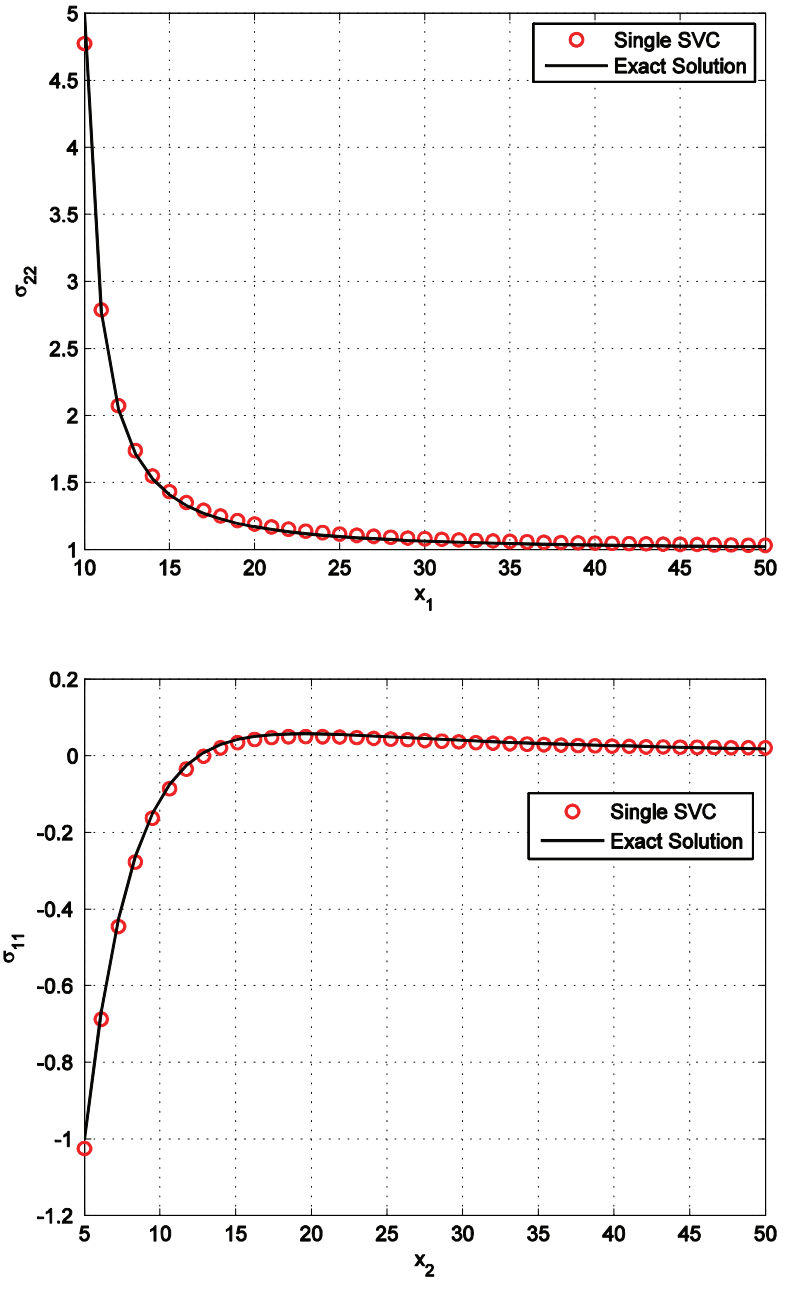

Figure 9: The computed σ_{11} along axis x_2 , and the computed σ_{22} along axis x_1 for the problem of an elliptical hole

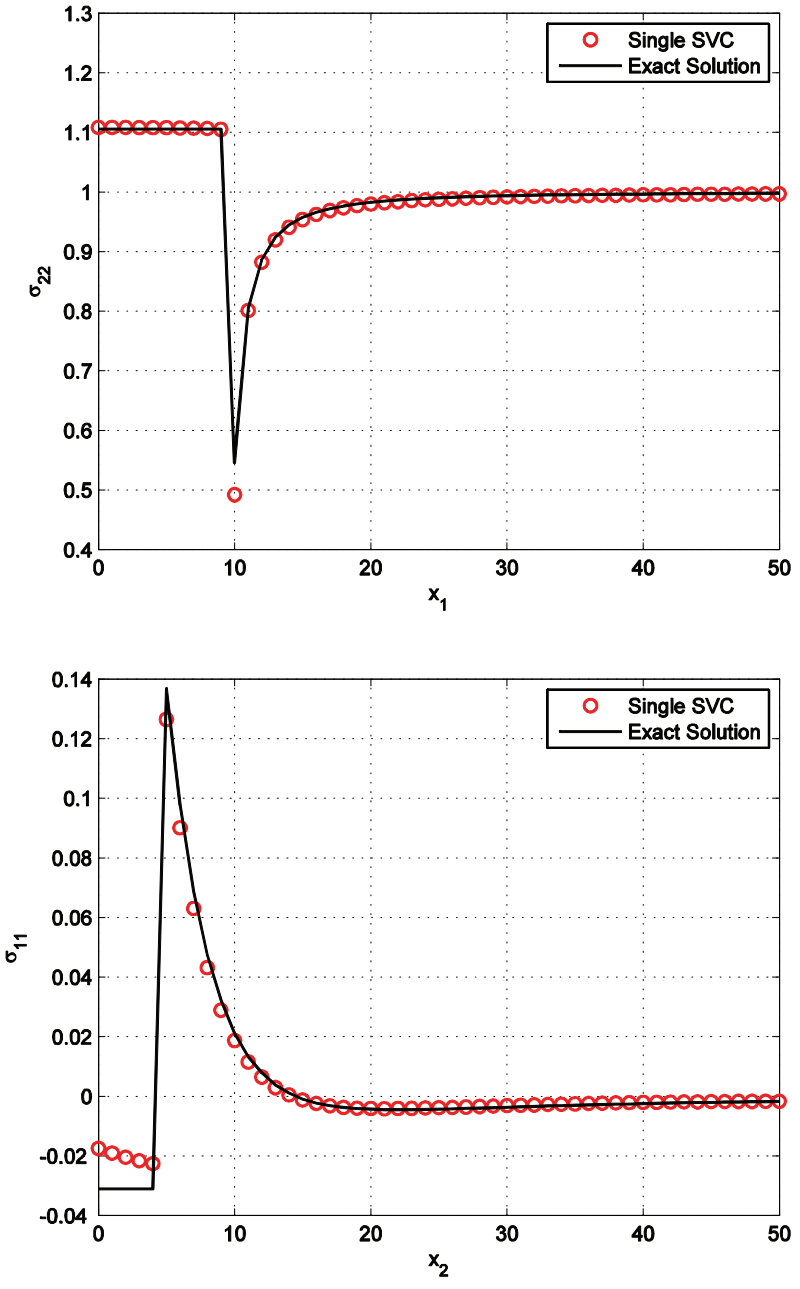

Figure 10: The computed σ_{11} along axis x_2 , and the computed σ_{22} along axis x_1 for the problem of an elliptical inclusion

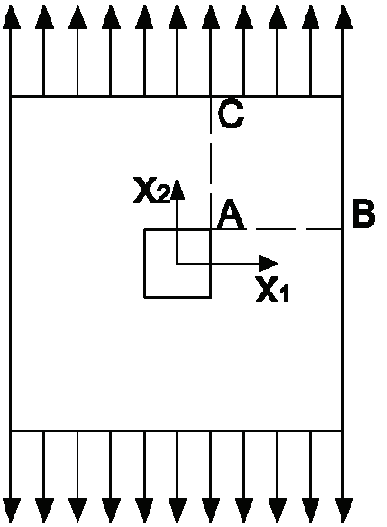

Figure 11: An infinite plate with a rectangular hole under remote tension

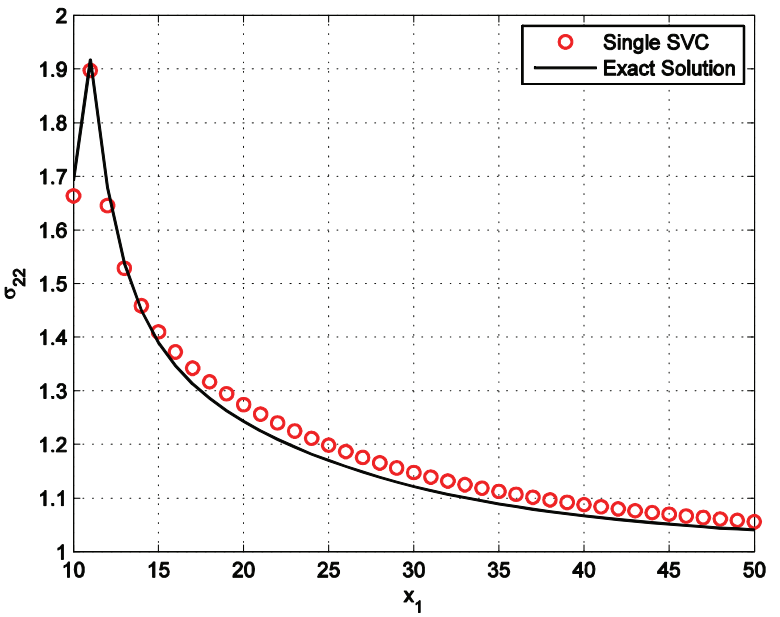

Figure 12: The computed σ_{22} along the line AB

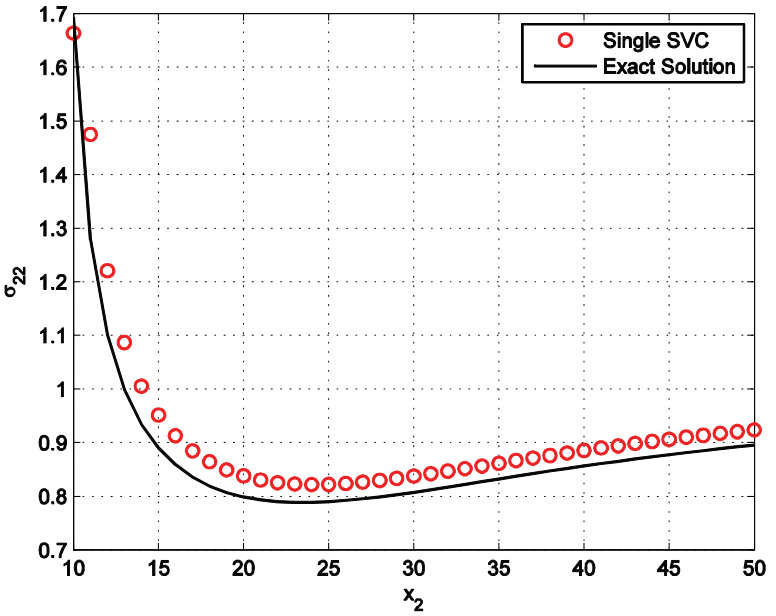

Figure 13: The computed σ_{22} along the line AC

Sidhu, and Ganesh (2006)], the present SVCs give much better results than the semi-analytical methods, even though a 2D RVE is used in this study.

The maximum principal stressand the strain energy density variations in the RVEs with different volume fractions of SiC are also computed and plotted in Fig. 16-21. While the inclusions are in a relatively uniform stress state, the stresses/strains vary rapidly in the Al matrix. To be more specific, very high stress level is observed near each corner of the polygon. Also,steep stress gradients are also observed in the Al material between the SiC particles, in the direction of loading. On the other hand, in the direction which is perpendicular to the direction of loading, relatively low stress values and strain energy density are observed.

It should be pointed out that, the very high accuracy of the computed stress/strain variations inan arbitrary heterogeneous material, is one of the major advantages of using the SVCs developed in this study, as compared to the VCFEMs developed by Ghosh and his coworkers in the past 15 years. Because high stresses/strains are indicators of damage-prone zones, and because SVCs are also very efficient and highly accurate for modeling arbitrary micro-crack and their non-collinear growth (as shown later), it is expected that SVCs are much more suitable for studying the damage development in composite materials, than VCFEMs.

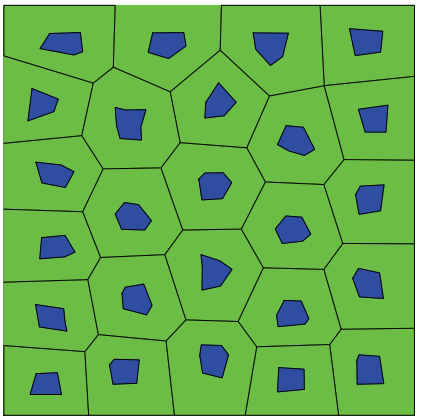

(a)

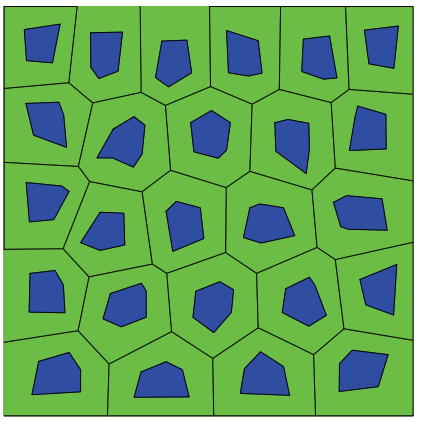

(b)

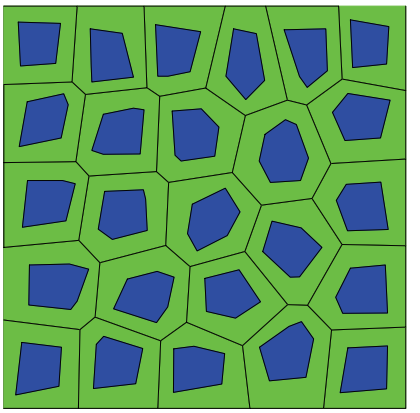

(c)

Figure 14: The RVEs of Al/SiC material with 25 polygonal inclusions, with different volume fractions of SiC: (a) 10% of SiC; (b) 20% of SiC; (c) 30% of SiC

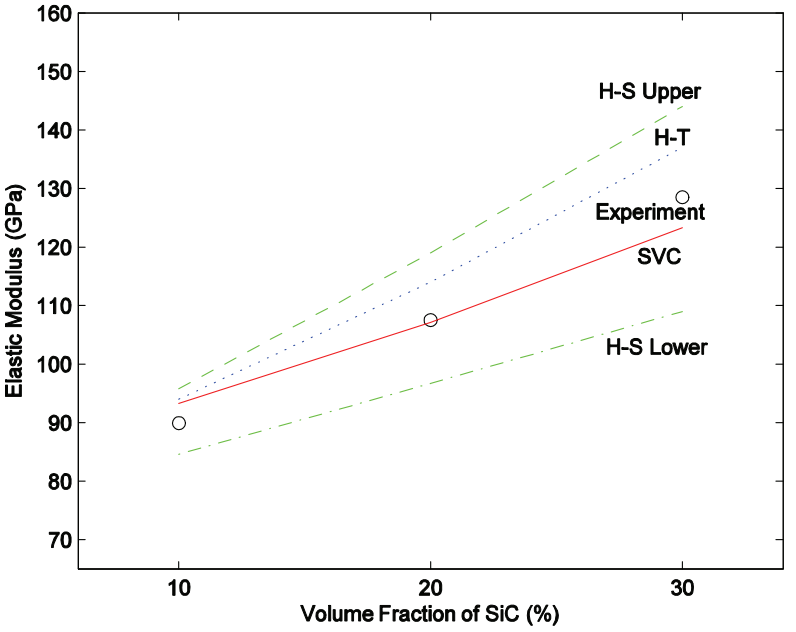

Figure 15: The computed stiffness of the Al/SiC material by the present SVCs, as compared to the Hanshin-Strikman upper and lower bounds, the Halpin-Tsai method, and the experimental results by [Chawla, Sidhu, and Ganesh (2006)]

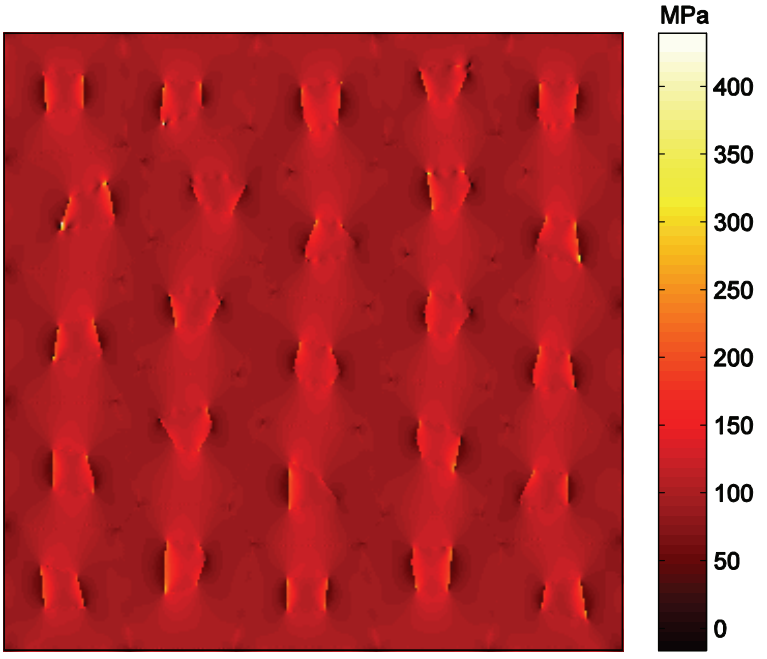

Figure 16: The distribution of maximum principal stress in the RVE of an Al/SiC material with 10% SiC

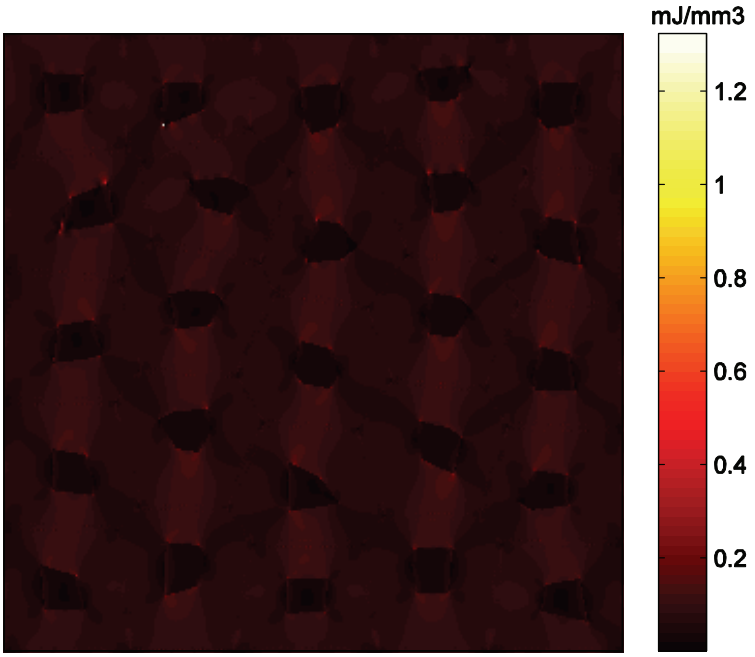

Figure 17: The distribution of strain energy density in the RVE of an Al/SiC materialwith 10% SiC

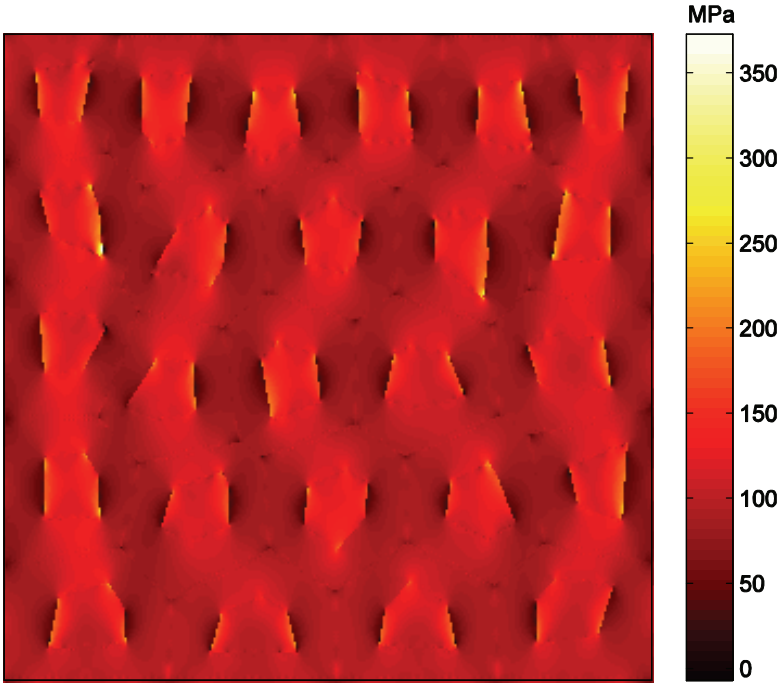

Figure 18: The distribution of maximum principal stress in the RVE of an Al/SiC materialwith 20% SiC

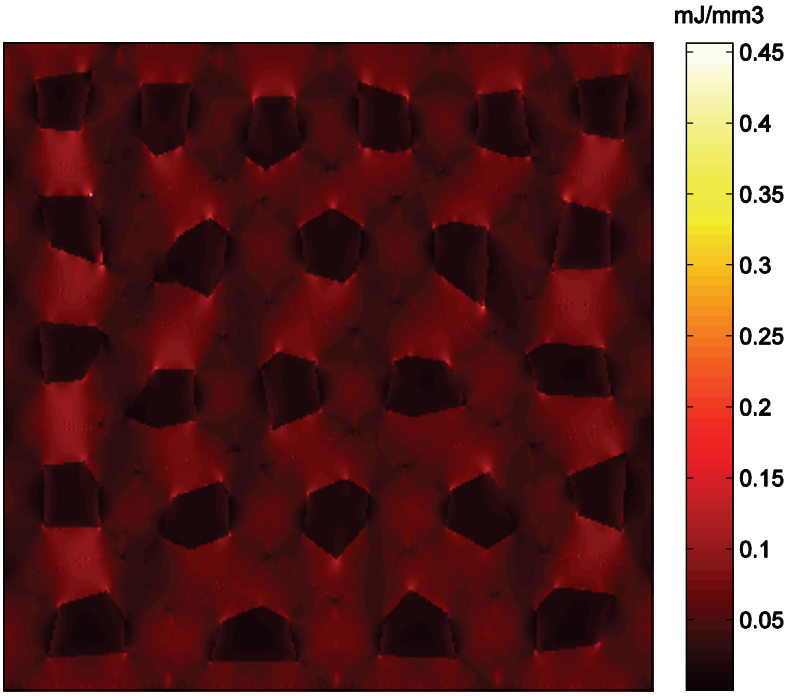

Figure 19: The distribution of strain energy density in the RVE of an Al/SiC materialwith 20% SiC

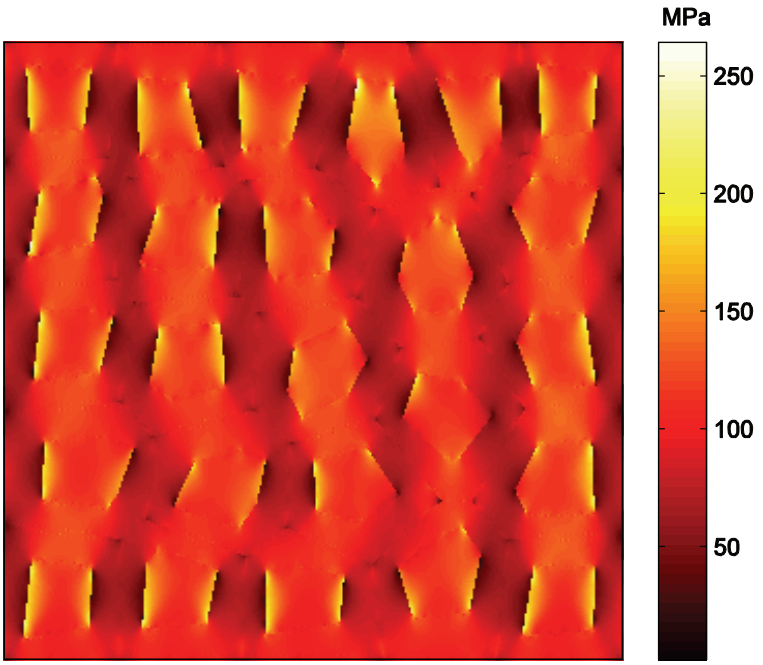

Figure 20: The distribution of maximum principal stress in the RVE of an Al/SiC materialwith 30% SiC

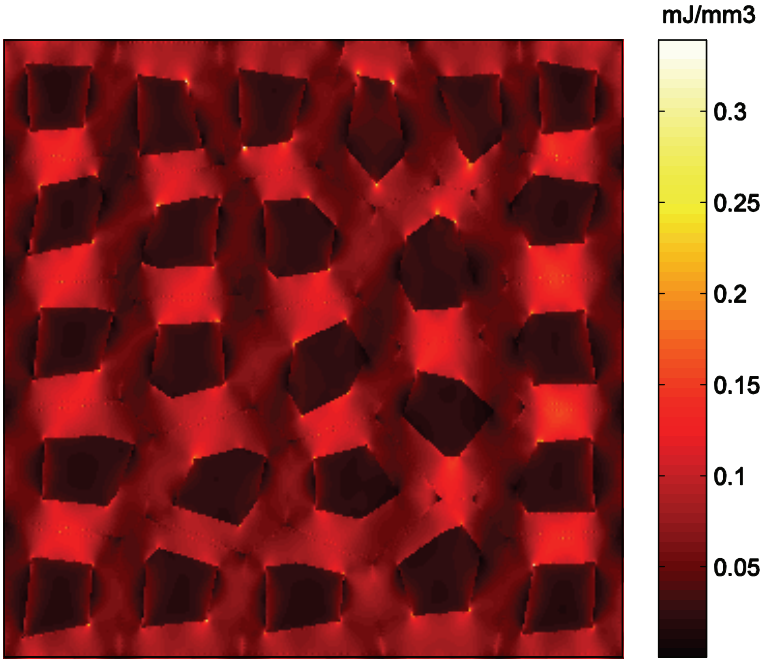

Figure 21: The distribution of strain energy density in the RVE of an Al/SiC materialwith 30% SiC

We also study the interaction between a micro-crack and an inclusion, see Fig. 22.A truncated 200×200 finite plate is considered. The radius of the inclusion is $r_v = 5$. The length of the crack is $2a_v = 10$. A plane strain condition is considered. The material properties of the matrix are $E_m = 1, v_m = 0.35$. The material properties of the inclusion are $E_c = 22.15, v_c = 0.3$. The center point of the crack is at (2.5, 10). ***A single SVC is used to solve this problem***. The boundary discretization of the SVC has 20 nodes at the outer boundary and 24 nodes at the matrix-inclusion interface, and 21 nodes for the crack. This example has been studied by [Huang, Liang and Yen (1995), Williams, Phan,Tippur, Kaplan and Gray (2007)]. In Tab. 1, we compare the presently computed normalized stress intensity factor, to the analytical solution:

$$F = \frac{K}{\sigma\sqrt{\pi a_v}} \tag{48}$$

Table 1: The stress intensity factors of the micro-crack near an inclusion

	A single SVC	Analytical
F1A	0.833	0.834
F2A	-0.062	-0.062
F1B	0.916	0.915
F2B	-0.052	-0.052

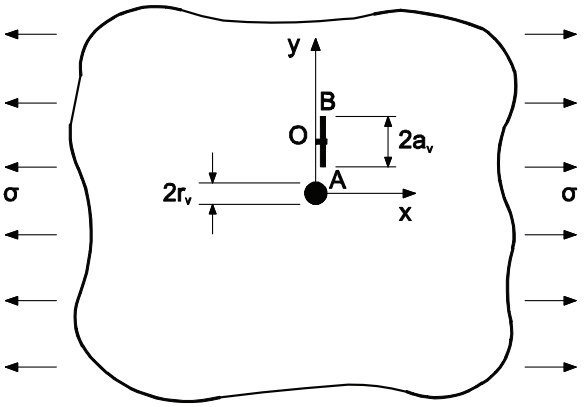

Figure 22: Crack / inclusion interaction in an infinite plate

In the next example, we model the fatigue growth of a crack passing an inclusion. The geometry of this problem is shown in Fig. 23. A 4×4 plate is considered. A circular inclusion with radius 0.25 is placed in the center. An edge crack with initial length 1.5 is considered. The material properties of the matrix are $E_m = 1, v_m = 0.3$. The material properties of the inclusion are $E_c = 3, v_c = 0.3$. A plane stress condition is considered. A uniform tension is applied to the upper and lower edges of the plate. ***A single SVC is used to solve this problem***. The boundary discretization of the SVC has 60 nodes at the outer boundary, 40 nodes at the matrix-inclusion interface, and 51 nodes for the crack. After fatigue growth, the crack is deflected by the inclusion, and then continues to grow into a mode 1 dominated crack, as shown in Fig. 24 and Fig. 25.

In a companion example, the same geometry shown in Fig. 23 is considered. However, this time a hole is considered instead of an inclusion. The material properties are $E = 1, v = 0.3$. Unlike the shielding effect of stiffer inclusion, the crack in this example eventually grows into the hole and stops, as can be seen in Fig. 26 and Fig. 27.

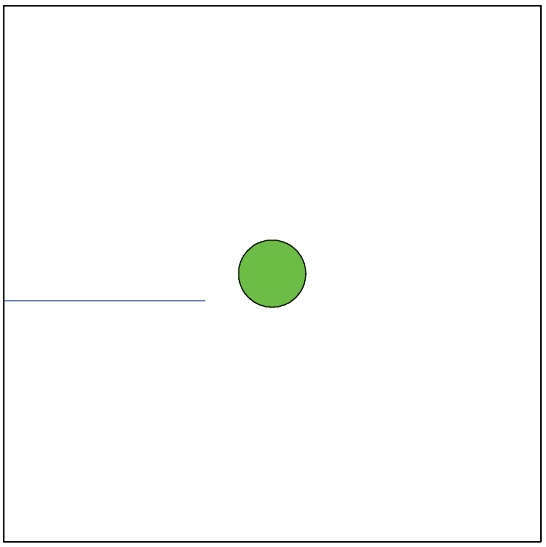

Figure 23: Initial crack near the inclusion or hole

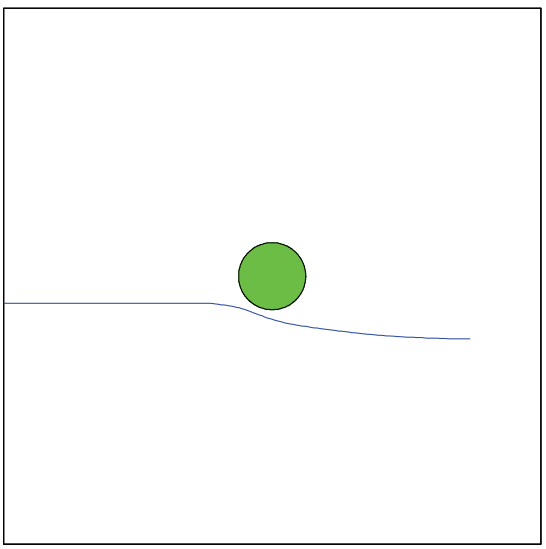

Figure 24: Final shape of the microcrack, after growing in fatigue, and after being deflected by the inclusion

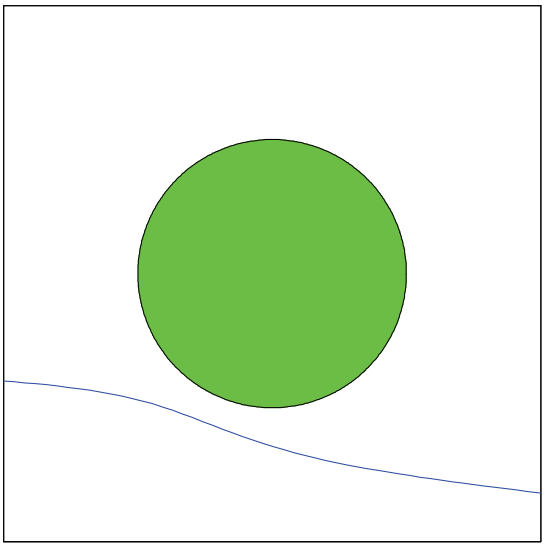

Figure 25: Close-up view of the final shape of the micro-crack, growing in fatigue, after being deflected by the inclusion

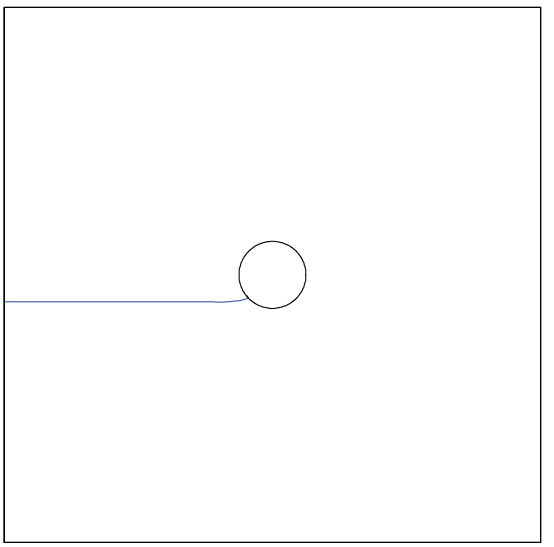

Figure 26: Final shape of the micro-crack, after fatigue: Crack grows into the void

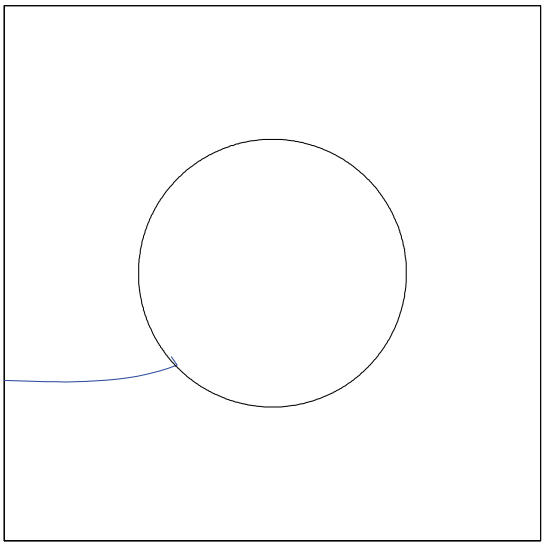

Figure 27: Close-up view of the microcrack, after growing under fatigue, after growing into the void

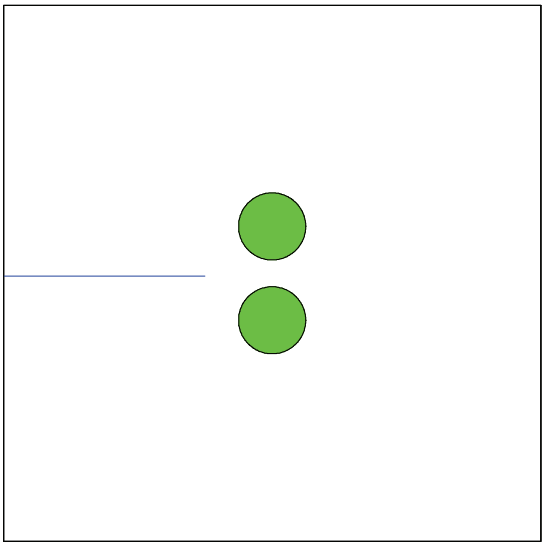

Figure 28: A slightly eccentric micro crack neartwo inclusions or two voids

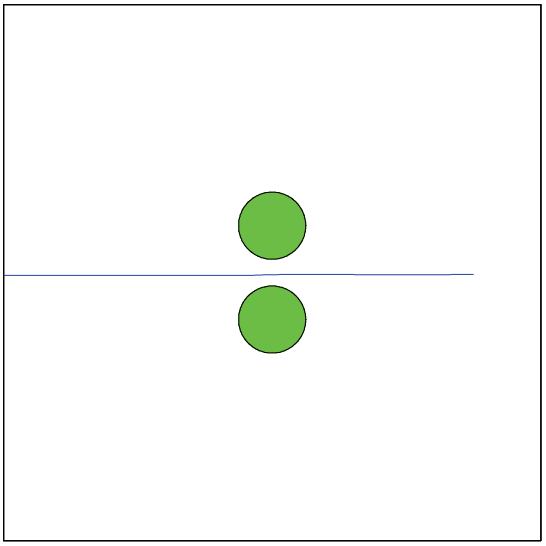

Figure 29: The final shape of the micro-crack, after growing under fatigue, and after passing through the two inclusions

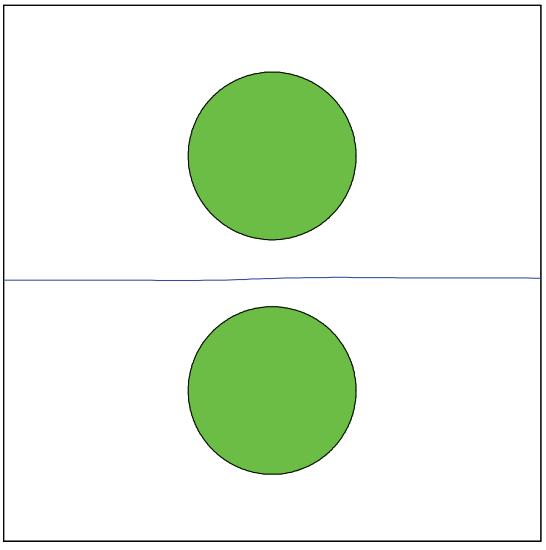

Figure 30: Close-up view of the micro- crack, after growing under fatigue, and after passing through the two inclusions

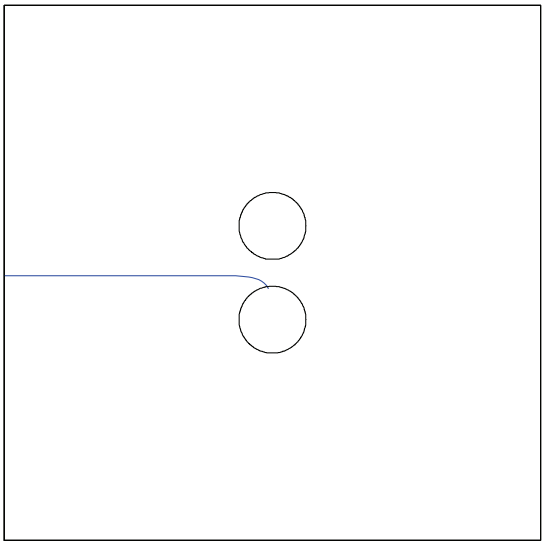

Figure 31: Final shape of the microcrack, after growing under fatigue, and after growing into one of the two holes

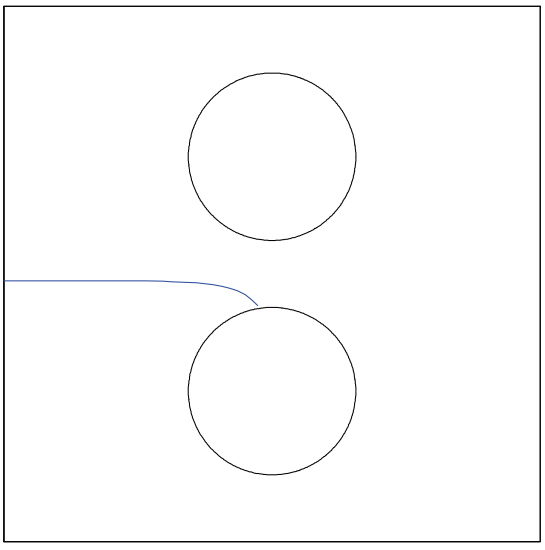

Figure 32: Close-up view of the micro- crack, growing under fatigue, and after growing into one of the two holes

In the next example, we model the growth of a crack near two inclusions or two holes. The geometry of this problem is shown in Fig. 28. A 4×4 plate is considered. Two circular inclusions or holes with radius 0.25 are placed symmetrically in the upper and lower part of the plate. The distance between the two inclusionsis 0.2. An edge crack with initial length 1.5 is considered. The crack is slightly closer to the lower hole or inclusion. The distance between the initial crack and the mid-line of the plane is 0.02. The material properties of the matrix are $E_m = 1, v_m = 0.3$. The material properties of the inclusion are $E_c = 3, v_c = 0.3$. A plane stress condition is considered. A uniform tension is applied to the upper and lower edges of the plate. ***A single SVC is used to solve this problem.*** The boundary discretization of the SVC has 60 nodes at the outer boundary, 40 nodes for each circular inclusion/hole, and 51 nodes for the crack.

After fatigue growth, the final crack shapes are shown in Fig. 29to Fig. 32. As can be seen clearly, the two stiffer inclusions push the crack back closer to the mid-line, and the crack successfully passes through the two inclusions. On the other hand, although the crack is only slightly eccentric, it grows into the nearer hole and stops.

After these benchmark examples of interactions of microcracks with inclusions and voids, we consider an example of microcrack growth in Al/SiC material. The RVE of Al/SiC, with 10% SiC is used, which is the same as the RVE in Fig. 14(a). Some microcracks are randomly generated in the RVE. As shown in Fig. 33, two cases are considered: (a), all microcracks are perpendicular to the loading direction; (b) microcracks are randomly inclined. The fatigue growth of these microcracks is considered, with a simple Paris Law: $da/dN = 6.9 \times 10^{-12} K^3$, with *Newton* and *mm* as units. After fatigue growth of microcracks, the final crack shapes and the principle stress/strain energy density of case (a) and case (b) are presented in Fig. 34-39. We see that, the fatigue growth of microcracksisclearly affected by the micro-structure: some cracks growth much faster than others. On the other hand, since the initial microcracks are very small, the inclination angle does not affect the final crack shape a lot.

6 Conclusions

By rearranging the weakly-singular boundary integral equations developed by [Han and Atluri(2003)], an SGBEM Voronoi Cell (SVC) is developed. The SVC, representing a single grain of a material, can include arbitrarily-shaped voids, inclusions (of a different material), and microcracks.The SVC has a stiffness matrix and a load vector, which have similar physical meanings to the traditional displacement FEM. The stiffness matrix is symmetric, positive-definite, and has the same number of rigid-body modes. Different SVCs, each with different isotropic material properties, can be directly coupled by the assembly procedure, and are used

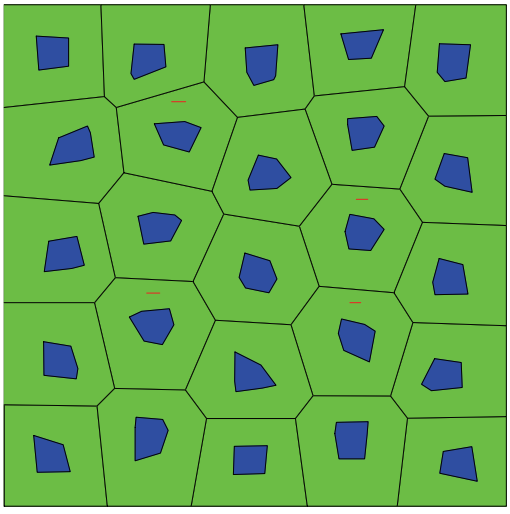

(a)

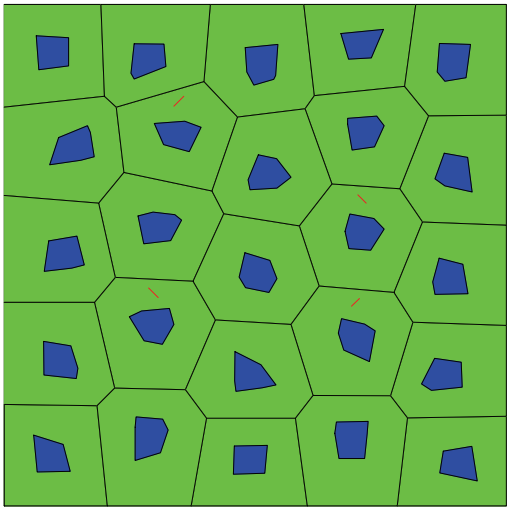

(b)

Figure 33: An RVE of Al/SiC material with 10% SiC, with: (a) horizontal microcracks; (b) inclined microcracks

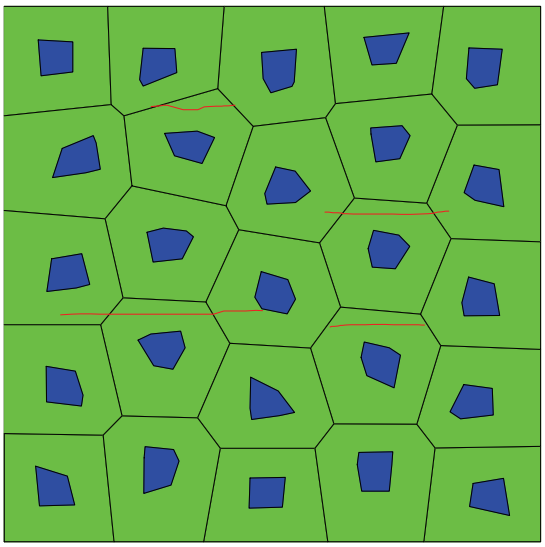

Figure 34: Final shapes of initially horizontal microcracks in Al/SiC material, after fatigue growth

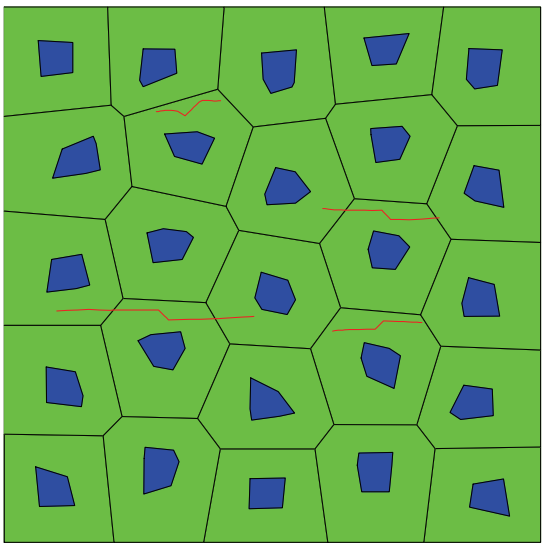

Figure 35: The final crack-shapes of initially inclined microcracks in Al/SiC material, after fatigue growth

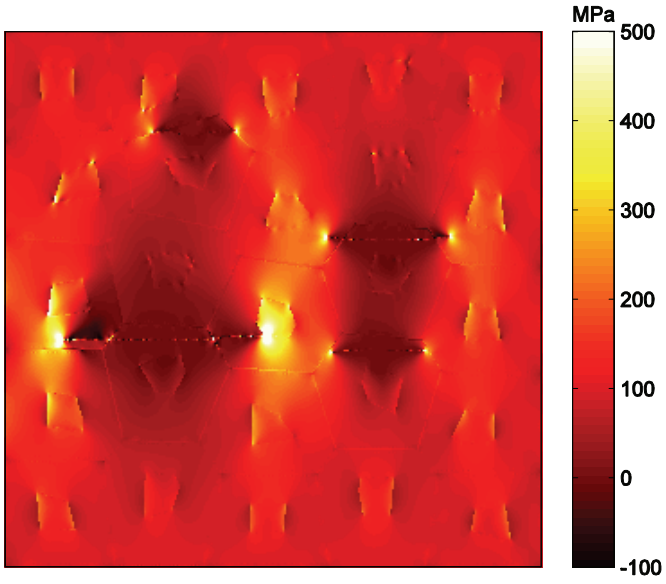

Figure 36: The distribution of maximum principal stress in an Al/SiC material with initially horizontal microcracks, after fatigue growth

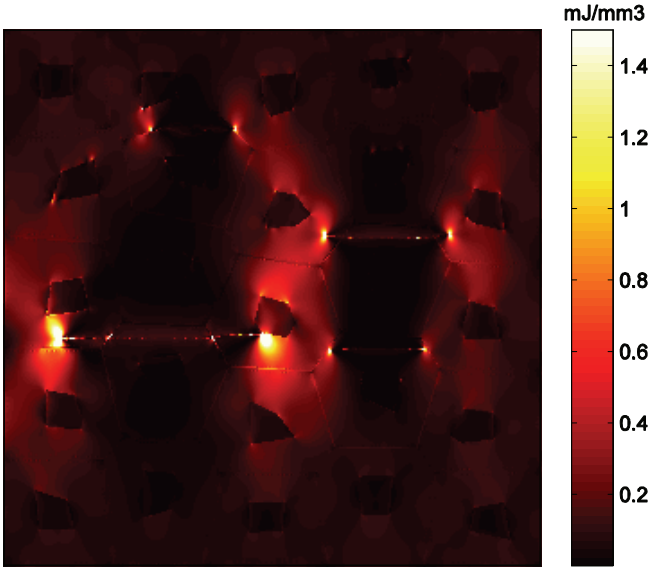

Figure 37: Distribution of strain energy density in Al/SiC material with initially horizontal microcracks, after fatigue growth

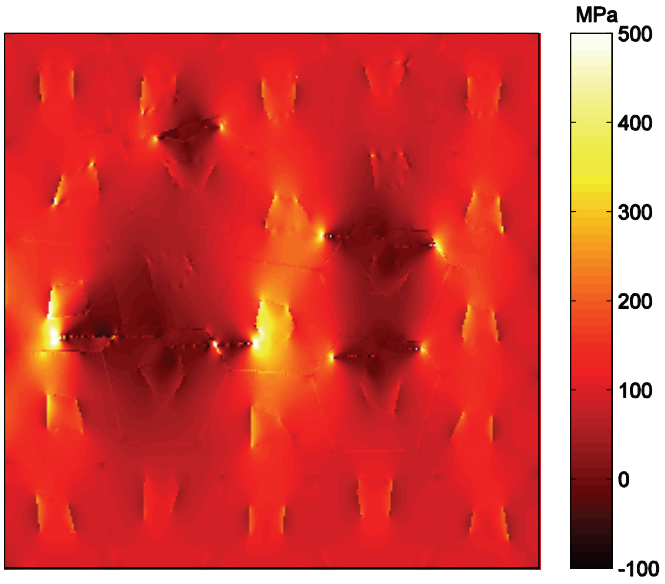

Figure 38: The distribution of maximum principal stress in an Al/SiC material with initially inclined microcracks, after fatigue growth

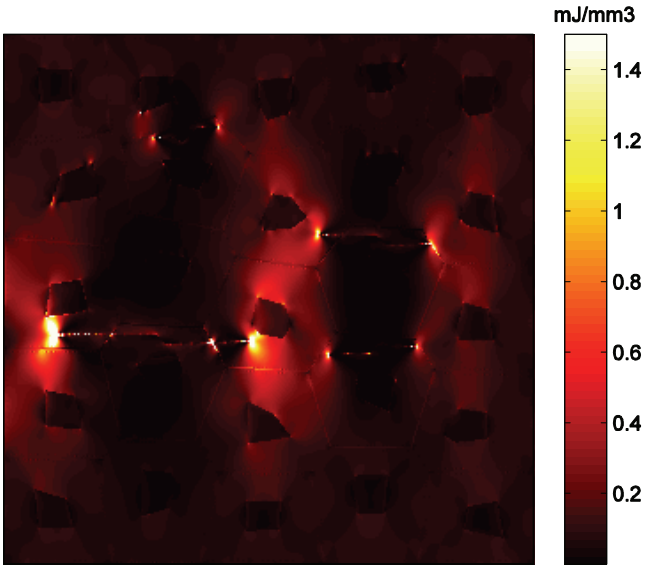

Figure 39: The distribution of strain energy density in an Al/SiC material with initially inclined microcracks, aftertheir fatigue growth

to directly and efficiently model the microstructure of heterogeneous composite materials. Some examples are also presented, with microcracks interacting with inclusions and holes. This provides some insight of a possible future study of the micro-cracking and damage of heterogeneous material.

By introducing stochastic variations of the shapes of SVC, and stochastic variations of the properties of the constituent materials, the realistic statistical bounds on the overall properties of composite materials will be determined in future studies.

Acknowledgement: This work was supported in part by the Vehicle Technology Division of the Army Research Labs, under a collaborative research agreement with University of California, Irvine (UCI). The encouragement of Dy Le and Jaret Riddick is thankfully acknowledged. The first author would like to thank Dr. Cheng Wang and Dr. Wen Chen for their support and advice.

References

Atluri, S.N. (2005): *Methods of Computer Modeling in Engineering and the Sciences, Vol. 1*, Tech Science Press.

Bao, G.; Hutchinson, J.W.; McMeeking, R.M. (1991): Particle reinforcement of ductile matrices against plastic flow and creep. *ActaMetallurgicaetMaterialia*, vol.39, no. 8, pp. 1871–1882.

Bonnet, M.; Maier, G.; Polizzotto, C. (1998): Symmetric Galerkin boundary element methods. *Applied Mechanics Review*, vol. 51, pp. 669-704.

Brezzi, F. (1974): On the existence, uniqueness and approximation of saddle-point problems arising from Lagrange multipliers. *Revue FrançaiseD'automatique, Informatique, RechercheOpérationnelle, AnalyseNumérique*, vol. 8, no. 2, pp. 129-151.

Bishay, P. L.; Atluri, S. N. (2012): High-Performance 3D Hybrid/Mixed, and Simple 3D Voronoi Cell Finite Elements, for Macro- & Micro-mechanical Modeling of Solids, Without Using Multi-field Variational Principles, *CMES: Computer Modeling in Engineering & Sciences*, vol. 84, no. 1, pp. 41-98.

Chawla, N.; Sidhu, R. S.; Ganesh, V. V. (2006): Three-dimensional visualization and microstructure-based modeling of deformation in particle-reinforced composites. *ActaMaterialia*, vol. 54, issue 6, pp. 1541-1548.

Christman, T.;Needleman, A.;Suresh, S.(1989): An experimental and numerical study of deformation in metal-ceramic composites. *ActaMetallurgica*, vol.37, no. 11, pp.3029-3050.

Dong, L.; Atluri, S. N. (2011a): A simple procedure to develop efficient &stable

hybrid/mixed VCs, and Voronoi Cell Finite elements for macro- &micromechanics. CMC: *Computers, Materials&Continua*, vol. 24, no. 1, pp.61-104.

Dong, L.; Atluri, S. N. (2011b): Development of Trefftzfour-node quadrilateral and Voronoi Cell Finite elements for macro- &micromechanical modeling of solids. CMES: *Computer Modeling in Engineering & Sciences*, vol.81, no. 1, pp.69-118.

Dong, L.; Atluri, S. N. (2012a): A simple multi-source-point Trefftzmethod for solving direct/Inverse SHM problems of plane elasticity in arbitrary multiply - connected domains. CMES: *Computer Modeling in Engineering & Sciences*, vol.85, no. 1, pp.1-43.

Dong, L.; Atluri, S. N. (2012b): T-TrefftzVoronoi Cell Finite Elements with eastic/rigid inclusions or voids for micromechanical analysis of composite and porous materials. CMES: *Computer Modeling in Engineering & Sciences*, vol.83, no. 2, pp.183-220.

Dong, L.; Atluri, S. N. (2012c): Development of 3D T-TrefftzVoronoi Cell Finite Elements with/without Spherical Voids &/or Elastic/Rigid Inclusions for Micromechanical Modeling of Heterogeneous Materials. CMC: *Computers, Materials & Continua*, vol. 29, no. 2, pp.169-212.

Dong, L.; Atluri, S. N. (2012d): Development of 3D TrefftzVoronoi Cells with Ellipsoidal Voids &/or Elastic/Rigid Inclusions for Micromechanical Modeling of Heterogeneous Materials. CMC: *Computers, Materials & Continua*, vol. 30, no. 1, pp.39-82.

Dong, L.; Atluri, S. N. (2013a): SGBEM (Using Non-hyper-singular Traction BIE), and Super Elements, for Non-Collinear Fatigue-growth Analyses of Cracks in Stiffened Panels with Composite-Patch Repairs. CMES: *Computer Modeling in Engineering & Sciences*, in press.

Dong, L.; Atluri, S.N. (2013b): Fracture & Fatigue Analyses: SGBEM-FEM or XFEM? Part 1: 2D structures. CMES: *Computer Modeling in Engineering & Sciences*, vol. 90, no. 2, pp. 91-146.

Dong, L.; Atluri, S.N. (2013c): Fracture & Fatigue Analyses: SGBEM-FEM or XFEM? Part 2: 3D solids. CMES: *Computer Modeling in Engineering & Sciences*, vol. 90, no. 5, pp. 379-413.

Eshelby, J. D. (1957): The determination of the elastic field of an ellipsoidal inclusion, and Related Problems. *Proceedings of the Royal Society A*, vol.241, pp.376-396.

Frangi, A; Novati, G. (1996): Symmetric BE method in two-dimensional elasticity: evaluation of double integrals for curved elements, *Computational Mechanics*, vol. 19, issue 2. pp. 58-68.

Frangi, A; Novati, G.; Springhetti, R.; Rovizzi, M. (2002): 3D fracture analysis by the symmetric Galerk in BEM, *Computational Mechanics*, vol. 28, pp. 220-232.

Ghosh, S.; Mallett, R. L. (1994): Voronoi cell finite elements. *Computers & Structures*, vol. 50, issue 1, pp. 33-46.

Ghosh, S.; Lee, K; Moorthy, S. (1995): Multiple scale analysis of heterogeneous elastic structures using homogenization theory and Voronoi cell finite element method. *International Journal of Solids and Structures*, vol. 32, issue 1, pp. 27-63.

Ghosh, S.; Lee, K; Moorthy, S. (2004): Three dimensional Voronoi cell finite element model for microstructures with ellipsoidal heterogeneties. *Computational Mechanics*, vol. 34, no.6, pp. 510-531.

Green, A. E.; Sneddon, I. N. (1950): The distribution of stress in the neighbourhood of a flat elliptical crack in an elastic solid. *Mathematical Proceedings of the Cambridge Philosophical Society,* vol. 46, issue 1, pp. 159-163.

Guedes, J. M.; Kikuchi, N. (1990): Preprocessing and postprocessing for materials based on the homogenization method with adaptive finite element methods. *Computer Methods in Applied Mechanics and Engineering*, vol. 83, issue 2, pp. 143-198.

Hashin, Z.;Shtrikman,S. (1963): A variational approach to the theory of the elastic behaviour of multiphase materials. *Journal of the Mechanics and Physics of Solids*, vol. 11, issue2, pp. 127-140.

Han, Z. D.; Atluri, S. N. (2003): On Simple Formulations of Weakly-Singular Traction & Displacement BIE, andTheir Solutions through Petrov-Galerkin Approaches. CMES: *Computer Modeling in Engineering & Sciences*, vol. 4, no. 1, pp.5-20.

Hill, R. (1965): Aself-consistent mechanics of composite materials. *Journal of the Mechanics and Physics of Solids*, vol. 13, no.4, pp. 213-222.

Hwu, C.; Liang, Y. K.; Yen, W. J. (1995).Interactions between inclusions and various types of cracks.*International journal of fracture*, vol. 73, no. 4, pp. 301-323.

Lei, C. M.; Ng. C. W. W.; Rigby, D. B. (2001): Stress and displacement around an elastic artificial rectangular hole, *Journal of Engineering Mechanics*, vol. 127, No. 9, pp. 880–890.

Li, R.;Chudnovsky, A. (1993): Energy analysis of crack interaction with an elastic inclusion.*International Journal of Fracture*, vol. 63, no. 3, pp. 247-261.

Li, S.; Mear, M.E.; Xiao, L. (1998): Symmetric weak form integral equation method for three-dimensional fracture analysis. *Computer Methods in Applied Me-*

chanics and Engineering, vol. 151, pp. 435-459.

Lipetzky, P.;Schmauder, S. (1994): Crack-particle interaction in two-phase composites Part I: Particle shape effects. *International Journal of Fracture*, vol. 65, no. 4, pp. 345-358.

Lipetzky, P.;Knesl, Z. (1995): Crack-particle interaction in a two-phase composite Part II: crack deflection.*International Journal of Fracture*, vol. 73, no. 1, pp. 81-92.

Lurie, A. I.(2005): *Theory of Elasticity*, 4^{th} edition, translated by Belyaev, Springer.

Moës.N.;Dolbow, J. O. H. N.;Belytschko, T. (1999).A finite element method for crack growth without remeshing.*International journal for numerical methods in engineering*, vol. 46, no. 1, pp. 131-150.

Muskhelishvili, N. I. (1954): *Some Basic Problems of the Mathematical Theory of Elasticity*, 4^{th} edition, translated by Radok, Noordhoff, Leyden, The Netherlands, 1975.

Nemat-Nasser, S.; Hori, M. (1999): *Micromechanics: Overall Properties of Heterogeneous Materials*, second revised edition, North-Holland.

Okada, H.; Rajiyah, H.; Atluri, S. N. (1988): A Novel Displacement Gradient Boundary Element Method for Elastic Stress Analysis with High Accuracy, *Journal of Applied Mechanics*, vol. 55, pp. 786-794.

Okada, H.; Rajiyah, H.; Atluri, S. N. (1989): Non-hyper-singular integral representations for velocity (displacement) gradients in elastic/plastic solids (small or finite deformations), *Computational Mechanics.*, vol. 4, no. 3, pp. 165-175.

Pian, T. H. H. (1964): Derivation of VC stiffness matrices by assumed stress distribution. *A. I. A. A. Journal*, vol. 2, pp. 1333-1336.

Savin, G. N (1961): *Stress Concentration around Holes*. Pergamon Press.

Sukumar, N.;Chopp, D. L.;Moës, N., Belytschko, T. (2001): Modeling holes and inclusions by level sets in the extended finite-element method. *Computer Methods in Applied Mechanics and Engineering*, vol. 190, no. 46, pp. 6183-6200.

Sun, C. T.;Vaidya, R. S. (1996).Prediction of composite properties from a representative volume element.*Composites Science and Technology*, vol. 56, no. 2, pp. 171-179.

Williams, R. C.; Phan, A. V.; Tippur, H. V.; Kaplan, T.; Gray, L. J. (2007): S-GBEM analysis of crack–particle(s) interactions due to elastic constants mismatch. *Engineering fracture mechanics*, vol. 74, no. 3, pp. 314-331.

Vijayakumar, K; Atluri, S. N. (1981): An embedded elliptical crack, in an infinite solid, subject to arbitrary crack-face tractions. *ASME, Journal of Applied Mechanics,* vol. 103, no. 1, pp. 88-96.